# Removal of $H_2S$ and $SO_2$ by $CaCO_3$-Based Sorbents at High Pressures

**Semiannual Report**

August 1997-January 1998

Prepared by:

**Prof. Stratis V. Sotirchos**

February 1998

Work Performed under Grant No.: DE-FG22-95PC95217

Performed for:

U.S. Dept. of Energy
University Coal Research Program
Pittsburgh Energy Technology Center
Pittsburgh, Pennsylvania

Performed at:

University of Rochester
Dept. of Chemical Engineering
Rochester, NY 14627

# Disclaimer

## EXECUTIVE SUMMARY

The theoretical and experimental investigation of the mechanism of $SO_2$ and $H_2S$ removal by $CaCO_3$-based sorbents (limestones and dolomites) in pressurized fluidized-bed coal combustors (PFBC) and high pressure gasifiers, respectively, is the main objective of this study. It is planned to carry out reactivity evolution experiments under simulated high pressure conditions or in high pressure thermogravimetric and, if needed, fluidized-bed reactor (high pressure) arrangements. The pore structure of fresh, heat-treated, and half-calcined solids (dolomites) will be analyzed using a variety of methods. Our work will focus on limestones and dolomites whose reaction with $SO_2$ or $H_2S$ under atmospheric conditions has been studied by us or other research groups in past studies. Several theoretical tools will be employed to analyze the obtained experimental data including a variable diffusivity shrinking-core model and models for diffusion, reaction, and structure evolution in chemically reacting porous solids.

During the six months of this reporting period, work was primarily done on the study of the behavior of the sulfidation of limestones under sequential calcination conditions in the presence of small amounts of oxygen and the development of a stochastic simulation code for determining the extent of pore volume trapping (formation of inaccessible pore space) in gas-solid reactions accompanied by pore volume reduction such as the sulfation and sulfidation of calcined limestones and dolomites.

The incentive for carrying out sulfidation experiments in the presence of oxygen was provided by the observation that some sulfidation experiments that were conducted as oxygen was accidentally leaking into the feed mixture of the reactor showed completely different behavior from that obtained in the absence of oxygen. Experiments were carried out in the thermogravimetric analysis system that we developed for studying gas-solid reactions at atmospheric or subambient pressures. The two $CaCO_3$ solids (Greer limestone and Iceland spar) that we employed in our previous experiments were used in the sulfidation

and calcination experiments, and the concentration of oxygen that was introduced in the $H_2S$-containing stream that was fed to the reactor ranged from 0.2 to 2.5%. The obtained results showed that the behavior of the sulfidation of limestone depended strongly, in both a qualitative and a quantitative sense, on the level of the oxygen concentration in the feed. For small oxygen concentrations, the weight gained by the calcined sample during sulfidation in a $N_2$-$H_2S$ atmosphere went through a maximum, whereas for oxygen concentrations above 0.5-0.6%, it increased continuously. A constant weight value was reached at large reaction times in both cases. The value of the weight gain at the maximum increased with increasing concentration of oxygen in the feed, and the same behavior was manifested by the constant value reached at large times. When a maximum was present in the weight gain vs. time curve, the constant value was lower than that expected for complete sulfidation of the solid. On the other hand, for oxygen concentration around 2-3%, the particles reached weight gains that corresponded to complete conversion of $CaO$ to $CaSO_4$ even though the maximum allowable conversion for complete pore plugging by $CaSO_4$ is about 50%.

The simulation scheme for studying inaccessible pore volume formation combines a gradual increase of the size of the grain that represent the porous structure with a random walk scheme, the latter used to determine whether a randomly chosen point in the unit cell of the two-phase structure lies in the particle phase or in the connected or isolated part of the matrix phase. The use of the algorithm was demonstrated by performing computations on structures of freely overlapping, unidirectional cylinders, and results were obtained both for the volume fractions and the specific surface areas of the accessible and inaccessible parts of the pore phase.

## TABLE OF CONTENTS

## LIST OF FIGURES

## 1. BACKGROUND INFORMATION

In a fluidized-bed combustor, a bed of combustible (coal) and noncombustible material is fluidized using air blown upward. Using dolomite or limestone as the noncombustible material, it is possible to have fuel combustion and flue gas desulfurization taking place simultaneously in the combustion vessel. If operation occurs under atmospheric pressure, the average partial pressure of carbon dioxide in the combustor (typically, 10-15% of the total pressure) is considerably lower than the equilibrium $CO_2$ pressure for decomposition of limestone ($CaCO_3$) or dolomite ($CaCO_3 \cdot MgCO_3$) at the temperatures usually encountered in FBC units (800-950 $^o$C). In the high temperature environment of the AFBC unit, the limestone or dolomite particles undergo calcination, yielding a highly porous product ($CaO$ or $MgO$), which reacts with the sulfur dioxide produced during coal combustion forming, mainly, calcium or magnesium sulfate. The sulfates occupy more space than the oxides they replace, and as a result, the pores of the calcine are completely plugged with solid product before complete conversion takes place. (The conversion for complete pore plugging is about 50% for the calcine of a stone consisting of $CaCO_3$ only.) Pores of different size are plugged at different conversion levels, and it is thus possible to have formation of inaccessible pore space in the interior of the particles when the small feeder pores of clusters of large pore are filled with solid product (Zarkanitis and Sotirchos, 1989). Moreover, under conditions of strong internal diffusional limitations, complete pore closure may first take place at the external surface of the particles while there is still open pore space left in the interior. For these reasons, ultimate conversions much lower than those predicted by the stoichiometry of the reaction for complete plugging of the internal pore space (less than 30-40%) are seen in AFBC units.

The reaction of calcined limestones (primarily) and dolomites with $SO_2$ has been the subject of extensive investigation. In accordance with the above remarks, the experimental evidence in most of the studies of the literature indicates strong effects of the pore size distribution on the overall reactivity of the calcined solids (Borgwardt and Harvey, 1972;

Wen and Ishida, 1973; Hartman and Coughlin, 1974, 1976; Ulerich et al., 1977; Vogel et al., 1977; Hasler et al., 1984; Simons and Garman, 1986; Yu, 1987; Gullett and Bruce, 1987; Zarkanitis and Sotirchos, 1989; Zarkanitis, 1991; Sotirchos and Zarkanitis, 1982). Unfortunately, the immense volume of information that has been accumulated over the years on the reaction of calcined limestones and dolomites with $SO_2$ is not applicable to $SO_2$ emissions control by limestones and dolomites under PFBC conditions. PFBC units normally operate under a pressure of 16 atmospheres, and for an average $CO_2$ content of 15%, this implies that the partial pressure of $CO_2$ in the reactor is 2.4 atm. Thermodynamic calculations show that the temperature for $CaCO_3$ calcination in the presence of 2.4 atm of $CO_2$ must be larger than $980^o$ C, that is, well above the temperature range (750-$950^o$ C) encountered in a PFBC unit. Nevertheless, even though formation of a highly porous material with a high specific surface area cannot take place under PFBC conditions, favorable desulfurization is known to occur in PFBC units (Bulewicz and Kandejer, 1986; Murthy et al., 1979). For dolomites, the situation is somewhat different since half-calcination (formation of an $MgO$-$CaCO_3$ product) is possible under 2.4 atm of $CO_2$. Even in this case, however, if the absorption of $SO_2$ occurred only in the pore space of the half-calcined solid, the utilization of the calcium content of dolomites should be much smaller than what is seen in practice under PFBC conditions.

The reaction of $CaCO_3$ with $SO_2$ may involve various reaction steps (Van Houte et al., 1981):

$$CaCO_3 + SO_2 \rightarrow CaSO_3 + CO_2 \tag{1}$$

$$CaSO_3 + \frac{1}{2}O_2 \rightarrow CaSO_4 \tag{2}$$

$$CaSO_3 + \frac{1}{2}SO_2 \rightarrow CaSO_4 + \frac{1}{2}S \tag{3}$$

$CaSO_3$ decomposes at temperatures higher than 650 $^o$C, and therefore, under typical operating conditions in a PFBC unit, the overall reaction may be written as:

$$CaCO_3 + SO_2 + \frac{1}{2}O_2 \rightarrow CaSO_4 + CO_2 \tag{4}$$

For dolomites, one should also address the question of the reaction of $MgO$ with $SO_2$.

If the partial pressure of $CO_2$ within the bed varies, calcination of $CaCO_3$ may take place in regions where $CO_2$ pressures lower than the equilibrium pressure are prevailing. The calcination of $CaCO_3$ will yield a partially calcined product, the extent of calcination depending on the residence time of the solid in the low $CO_2$ concentration region. $CaO$ formed in the solid will react with the $SO_2$ present in the bed in the same fashion as in the case of AFBC units:

$$CaCO_3 \rightarrow CaO + CO_2 \tag{5}$$

$$CaO + SO_2 + \frac{1}{2}O_2 \rightarrow CaSO_4 \tag{6}$$

If the partially calcined solid moves into regions rich in $CO_2$, where reaction (5) is favored to proceed from right to left, carbonation, i.e., recovery of $CaCO_3$, will take place, with reaction (4) competing with reaction (5) for $CaO$. Decomposition of $CaCO_3$ may also take place even if there is no variation of the $CO_2$ pressure in the reactor. Large variations in the temperature profile (100-140$^o$ C) within the combustor unit have been reported by Smith et al. (1982). Therefore, if the solid particles move into regions where the temperature of the reactor is above the temperature at which $CaCO_3$ is stable, at the average partial pressure of $CO_2$ in the reactor, decomposition of $CaCO_3$ will occur. However, only small amounts of $CaO$ have been found in the reactor by Ljungstrom and Lindqvist (1982), suggesting that direct sulfation of limestones (eq. (4)) is the main reaction occurring in the combustor. Similarly, PFBC data from Exxon (Hoke et al., 1977) with uncalcined Grove limestone showed that most of the unreacted $Ca$ in the bed for $CO_2$ partial pressures above the equilibrium value existed in the form of $CaCO_3$.

Studies of $SO_2$ removal at high pressures have been carried out both with carbonates and precalcined solids (Newby et al., 1980; Ulerich et al., 1982; Dennis and Hayhurst, 1984, 1987; Bulewicz et al., 1986). However, because of the aforementioned complexities, with the exception of the general conclusion that favorable desulfurization is possible under PFBC conditions, there is not much agreement in the literature on the effects of the various

parameters on the process. Dennis and Hayhurst (1984, 1987), for example, found that the reaction rate of precalcined limestones in a fluidized-bed reactor decreases with an increase in the operating pressure, both in the absence and presence of $CO_2$. Working with a laboratory-size PFBC, Bulewicz et al. (1986) observed an increase in the sorption capacity of $Ca$-based sorbents (chalk, limestone, and dolomite) with an increase in pressure up to 2 atm, but further increase in pressure caused a reduction in the sorption capacity of all samples. Similar observations were made by Jansson et al. (1982). PFBC studies at Exxon (Hoke et al., 1977) showed better sulfur retention for precalcined limestones, but Stantan et al. (1982) observed no improvement in sorbent utilization by precalcination. Stantan et al. also reported that under weakly noncalcining conditions, a feed of uncalcined limestone gave better sulfur retention than what kinetic studies performed in a thermogravimetric apparatus predicted.

A situation similar to that prevailing in PFBC units is encountered in desulfurization in gasifier at high pressures. Fixed-bed and fluidized-bed gasifiers typically operate around 850 $^o$C with a temperature at the exit of around 500-800 $^o$C. The pressure of operation is in most cases in the 200-300 psi range, and at an average pressure of 250 psi, it turns out that the $CO_2$ partial pressure in the reactor is about 1.8 and 4.3 atm for air blown and oxygen blown gasifiers, respectively (based on a typical $CO_2$ content (mole/mole) of 11% and 26%, respectively (Grindley et al., 1985). Almost all observations made for $SO_2$ removal in PFBC reactors apply to $H_2S$ removal in high pressure gasifiers but with reactions (7) and (8) taking place (primarily) in a gasifier instead of (4) and (6):

$$CaCO_3 + H_2S \rightleftharpoons CaS + CO_2 + H_2O \tag{7}$$

$$CaO + H_2S \rightleftharpoons CaS + H_2O \tag{8}$$

Like in the case of sulfation, the main difference between the direct and indirect reactions is that a highly porous solid is involved in the indirect process while that participating in the direct reaction is essentially nonporous. In view of this difference, the information that is

presently available on the sulfidation of limestone-derived calcines (e.g., see Borgwardt et al. (1984) and Efthimiadis and Sotirchos (1992)) and sulfidation of half-calcined dolomites (e.g., see Ruth et al. (1972) and Yen et al. (1981)) from studies in thermogravimetric analysis (TGA) systems and other types of reactors is inapplicable to the direct reaction of limestones with $H_2S$. Few fundamental studies have been presented in the literature on the direct reaction of limestones with $H_2S$, and most of those have been carried out under low pressures (Borgwardt and Roache, 1984) or under conditions where both sulfidation reactions ((7) and (8)) could take place (Attar and Dupuis, 1979).

The direct sulfation or sulfidation of calcium carbonate-containing sorbents can be studied under atmospheric pressure provided that there is enough $CO_2$ in the reactor to prevent decomposition of the carbonate (simulated PFBC or high pressure gasification conditions). Tullin and Ljungstrom (1989) performed sulfation experiments in a thermogravimetric analyzer (TGA) under conditions inhibiting calcination of $CaCO_3$ and found that the sulfation rate of uncalcined $CaCO_3$ was comparable with the sulfation rate of calcined material; they thus concluded that desulfurization in PFBC's is achieved by direct sulfation of limestones. Large amounts of sample and small particles (around 150 mg and 10-90 $\mu$m) were used by those authors in their experiments, and thus extracting any quantitative information is practically impossible (because of strong interparticle diffusional limitations). A similar procedure was employed by Snow et al. (1988) and Hajaligol et al. (1988), who also observed that the direct sulfation of $CaCO_3$ can reach for some precursors higher conversions than the sulfation of the calcines ($CaO$). High concentrations of $CO_2$ (70% $CO_2$ by volume) were also used by Borgwardt and Roache (1984) to study the direct reaction of limestone particles with $H_2S$ at atmospheric pressure in a differential reactor. They employed a limestone precursor (Fredonia limestone) of relatively high porosity (about 8%), and thus, they were able to explain the behavior of the conversion-time trajectories for large particles (diameter greater than 15 $\mu$m) along the lines of the overall mechanism for the sulfidation of limestone-derived calcines (reaction (8)).

A detailed investigation of the direct sulfation of limestones with $SO_2$ and $H_2S$ under simulated high pressure conditions was carried out by my research group (Krishnan and Sotirchos, 1993a,b,1994) using three limestone specimens of high $CaCO_3$ content. In accordance with the observations of Tullin and Ljungstrom (1989), Snow et al. (1988), and Hajaligol et al. (1988), our sulfation results (Krishnan and Sotirchos, 1993a,1994) showed that the direct reaction of calcium carbonate with $SO_2$, believed to be the dominant reaction in a PFBC, is qualitatively different from the reaction of limestone calcines. A similar conclusion was reached for the limestone-$H_2S$ reaction (Krishnan and Sotirchos, 1994). These results reinforced our early conclusion that the accumulated knowledge in the literature from the extensive study of the reaction of calcined limestones and dolomites with $SO_2$ or $H_2S$ cannot be used to derive any reliable conclusions for flue or coal gas desulfurization under high pressure conditions. Nevertheless, with the exception of the studies conducted under simulated high pressure conditions on a few limestones, no fundamental studies have been carried out in the literature on the reaction of limestones and dolomites with $SO_2$ or $H_2S$ under true high pressure conditions (i.e., at high pressures and in the presence of $CO_2$). Moreover, even though the experimental data under simulated high pressure conditions have been extremely helpful in elucidating some of the phenomena encountered in the direct sulfation or sulfidation of limestones, it is questionable whether these results are directly applicable to reaction under true PFBC or high pressure gasification conditions, especially for solids with significant dolomitic content.

Based on the above observations, a research program has been proposed for the investigation of the mechanism of $SO_2$ and $H_2S$ removal by limestones and dolomites at high pressures. Reactivity evolution experiments will be carried out using thermogravimetric and, if needed, fixed-bed and fluidized-bed reactor (high pressure) arrangements. Thermogravimetric experiments will be carried out under simulated high pressure conditions at atmospheric pressure using a unit currently available in our lab and at high pressures using a high pressure TGA proposed to be set up under this project. The pore structure

of fresh, heat treated, and half-calcined solids (dolomites) will be analyzed using a variety of methods. Our work will focus on limestones and dolomites whose reaction with $SO_2$ or $H_2S$ under atmospheric conditions has been in detail investigated by either us or other research groups. The obtained experimental data will be analyzed using various theoretical tools developed by my research group for studying gas-solid reactions, and will be used as basis for the development of predictive single particle models for use in design models of combustors or gasifiers.

## 2. WORK DONE AND DISCUSSION

During the six months of this reporting period, work was primarily done on the study of the behavior of the sulfidation of limestones under sequential calcination conditions in the presence of small amounts of oxygen and the development of a stochastic simulation code for determining the extent of pore volume trapping (formation of inaccessible pore space) in gas-solid reactions accompanied by pore volume reduction such as the sulfation and sulfidation of calcined limestones and dolomites. More information on the work done is provided below.

### 2.1. Sulfidation of Calcined Limestones in the Presence of Oxygen

Some sulfidation experiments, under sequential or simultaneous conditions, were carried out in the presence of accidental leaks of small amounts of oxygen into the feed mixture of the reactor. These experiments showed completely different behavior from that obtained in the absence of oxygen. Specifically, after an initial weight gain, precalcined samples experienced weight loss that led to final weights that were below the values that were expected for complete sulfidation. On the other hand, samples that were subjected to simultaneous sulfidation and calcination showed continuous decrease of weight reaching final weights that were only slightly higher than those expected for complete calcination without further reaction. These results suggested that in the presence of small amounts of oxygen – as it is the case in a gasifier – the behavior of the limestone particles could

be much different from that inferred from successive or sequential calcination and sulfidation experiments. It was thus decided to investigate the phenomenon by carrying out sulfidation experiments on precalcined limestones in the presence of small concentrations of oxygen in the feed of known value.

Experiments were carried out in the thermogravimetric analysis that we have set up in our laboratory under this project for gas-solid reactions at subambient or atmospheric pressure. As in the previous studies, samples obtained from limestones of high calcium carbonate content (¿ 95%) were employed in the experiments. In order to avoid having significant interparticle diffusional limitations, a small amount of solid (1.5-4 mg) was used for reactivity experiments. Gas flow rates of 200 ml/min under standard conditions were used in all of the experiments. The samples were brought to the reaction temperature under $CO_2$ to prevent their decomposition, and calcination was carried out by replacing the $CO_2$ stream with air. For sulfidation we employed a steam of 7,000 ppm $H_2S$ in $N_2$, in which we added small amounts of $O_2$.

Some of the obtained results for 53-62 $\mu$m Greer limestone particles are shown in Figures 1-3. The reactivity vs. time data are presented as the ratio of the weight of the sample at time $t$, $W_t$, to the initial weight, $W_0$, vs. time. To make the graphs directly comparable with those presented in previous reports, the results for sulfation are presented as the weight gain added to the initial weight of the limestone before calcination. It follows from the results of Figures 1-3 that the behavior of the sulfidation of limestone depends strongly, in both a qualitative and a quantitative sense, on the level of the oxygen concentration in the feed. For small concentration of oxygen (Figure 1), the weight gained by the calcined sample during sulfidation in a $N_2$-$H_2S$ atmosphere goes through a maximum, whereas for concentrations above 0.5-0.6% (Figures 2 and 3), it increases continuously. The weight change appears to level off at large reaction times in both cases. The value of the weight gain at the maximum increases with increasing concentration of oxygen in the feed, and the same behavior is exhibited by the constant value reached at large times.

The weight change of the sample at large reaction times in Figure 1 (that is, when a maximum is present in the weight gain vs. time curve) is lower that the value that is expected for complete sulfidation of the solid – which is what happens when the reaction is carried in the absence of oxygen. This suggests that part of the sulfide is converted back to oxide, most probably through the reaction of $CaS$ with $CaSO_4$ formed from the oxidation of $CaS$. This reaction has been studied by several investigators, mainly in the context of stabilization, by oxidation to $CaSO_4$, of $CaS$ formed during $H_2S$ removal in coal gasifiers using limestones or dolomites (e.g., Abbasian et al. (1991), Davies et al. (1994), Van der Ham et al. (1996), and Yrjas et al. (1996)). Since the solid sample is continuously exposed to $H_2S$, the leveling off of the weight gain to values at which $CaO$ must be present indicates that the $CaO$ that is formed from the solid-solid reaction of $CaS$ and $CaSO_4$ exhibits very low reactivity with $H_2S$. It is planned to test this conclusion by sulfiding completely precalcined limestones samples, oxidizing part of the sulfide to $CaSO_4$, forcing the solid-solid reaction to occur by raising the temperature, and, after completion of the solid-solid reaction takes place, exposing the samples to a mixture of $H_2S$-$N_2$.

For oxygen concentrations above 0.5-0.6% (Figures 2 and 3), the rate of $CaSO_4$ formation from the oxidation of $CaS$ is apparently much higher than that of $CaO$ formation from the solid-solid reaction of $CaS$ and $CaSO_4$, and as a result, the weight of the sample increases continuously in the course of the reaction. For oxygen concentration around 2.3% in Figure 2, the weight gain reached by the sample corresponds to complete conversion of $CaO$ to $CaSO_4$. This is a surprising result, since if the particle size does not change, the maximum conversion that can be reached for complete pore filling with $CaSO_4$ is about 50%. We are thus led to conclude that when calcined limestone particles react with $H_2S$ in the presence of oxygen, their size changes (increases) in the course of the reaction. As the temperature is changed from 750 to 850 $^o$C (see Figure 3), the weight gain of the particles for 2.3% $O_2$ in the feed decreases at all reaction times. A possible reason for this behavior could be the stronger intraparticle diffusional limitations at the higher reaction

temperature.

The results of Figures 1-3 are of great importance for the in situ removal of $H_2S$ in gasifiers through limestone injection since they show that even small amounts of oxygen can lead to completely different behavior of the limestone particles from that revealed by simultaneous or sequential calcination and sulfidation experiments. We intend to do more work on limestone sulfidation in the presence of oxygen in the next six-month period. Since in the presence of oxygen, $H_2S$ reacts in the gas phase to form other sulfur-containing species, we will perform thermodynamic equilibrium computations on the mixture fed to the chemical reactor to see what species are in existence at equilibrium in the gas phase at the reaction temperature. These results are expected to be of great help in explaining the behavior of the limestone sulfidation process in the presence of small concentrations of oxygen.

### 2.2. Development of a Simulation Scheme for Studying Volume Trapping in Reacting Grain Structures

A stochastic simulation scheme was formulated for studying matrix volume trapping in structures of growing particles, where growth can occur only on surfaces that serve as boundaries of infinite (accessible) subsets of the matrix phase. This is the case that is encountered in the sulfidation or the sulfation of calcined limestones. The following steps are involved in the method: i) a unit cell is constructed for the starting (mother) structure, and the mother structure is used as basis for the construction of a number of derivative (daughter) structures of uniformly grown particles; ii) a number of points is selected randomly within the unit cell, and these points are used as starting points of random walkers that travel in the matrix space (outside the particles) by suffering diffuse reflections (according to the cosine law) on the particle surfaces; iii) such computations are carried out both for the initial and the derivative structures, and the information that is extracted from these computations is employed to determine, for each uniformly grown

structure, which of the randomly selected points in the two-phase medium lie in the particle phase, the accessible part of the matrix, or its inaccessible part; iv) the same determination is made for the real particle structures (that is, with matrix volume trapping accounted for) using a method developed in this study, and this information is further employed to estimate matrix volume fractions, mean intercept lengths, surface areas, and volume and surface area distributions of matrix phase fragments. In addition, we develop a formula that allows us to determine the variation of the inaccessible matrix volume of the real structures with the extent of particle growth from the variation of the surface areas and volume fractions of the inaccessible and accessible parts of the uniformly grown structures. The obtained results for the real structures are approximate, converging to the exact results as the steps between successive structures approach zero.

The method was applied to structures of randomly overlapping (fully penetrable), unidirectional cylinders. The comparison of the results for real and uniformly grown structures showed that the inaccessible and total matrix volume fractions increase by relatively small amounts when formation of trapped matrix (pore) space is taken into account. Since the inaccessible matrix fragments tend to have much larger surface area per unit volume than the accessible matrix space (by about a factor of 4 at the onset of formation of inaccessible matrix space starts), the total surface area of real structures is slightly larger than that of uniformly grown structures of the same particle size. It is believed that the reason for the existence of small differences between real (with volume trapping accounted for) and uniformly grown structures is that formation of inaccessible matrix space occurs at a significant rate only close to the percolation threshold. In past studies, this was also observed to be the case for structures of multidirectional, randomly overlapping fibers or unidirectional, partially overlapping fibers. It is thus expected that real and uniformly grown structures will exhibit small differences for these cases as well. This is a very important result for since it implies that the information that is available in the literature on the percolation behavior of the above fibrous media for uniform fiber growth can also

be employed, without leading to significant errors for practical purposes, for the physically meaningful case where the fibers grow only on their accessible surfaces. This may also be the case for the grain or pore structures that are used to simulate the structure of calcined limestones (Yu, 1987; Sotirchos and Zarkanitis, 1992).

More information on this work can be found in the paper that is attached as an appendix to this report.

## 3. SUMMARY AND CONCLUSIONS

During the six months of this reporting period, work was primarily done on the study of the behavior of the sulfidation of precalcined limestones in the presence of small amounts of oxygen and the development of a stochastic simulation code for determining the extent of pore volume trapping (formation of inaccessible pore space) in gas-solid reactions accompanied by pore volume reduction, such as the sulfation and sulfidation of calcined limestones and dolomites.

Sulfidation experiments in the presence of oxygen were carried out because we had observed that leaks of oxygen into the feed mixture led to completely different results from those obtained in the absence of oxygen. The obtained results showed that the behavior of the sulfidation of limestone depended strongly, in both a qualitative and a quantitative sense, on the level of the oxygen concentration in the feed. For small concentration of oxygen, the weight gained by the calcined sample during sulfidation in a $N_2$-$H_2S$ atmosphere presented a maximum, whereas for concentrations above 0.5-0.6% , it increased continuously, reaching in some cases values that corresponded to complete conversion of $CaO$ to $CaSO_4$.

The simulation scheme for studying inaccessible pore volume formation combines a gradual increase of the size of the grains that represent the porous structure with a random walk scheme, the latter used to determine whether a randomly chosen point in the unit cell

of the two-phase structure lies in the particle phase or in the connected or isolated part of the matrix phase. The use of the algorithm was demonstrated by performing computations on structures of freely overlapping, unidirectional cylinders, and results were obtained both for the volume fractions and the specific surface areas of the accessible and inaccessible parts of the pore phase.

For the next reporting period we plan to do some more work on the process of limestone sulfidation in the presence of small quantities of oxygen. Some of the difficulties that we have been experiencing with the microfurnace arrangement of the high pressure TGA system have been resolved, and thus, experiments will be carried out both at atmospheric and high pressures. High pressure experiments will also be done on limestone sulfation and limestone sulfidation in the absence of oxygen. Finally, we plan to complete the analysis of the experimental data that we have obtained using the mathematical model for simultaneous decomposition and solid product formation reactions we have developed.

## BIBLIOGRAPHY

Abbasian, J., A. Rehmat, and D.D. Banerjee, Ind. Eng. Chem. Res., 30, 1990-1994 (1991).

Attar, A., and F. Dupuis, Ind. Eng. Chem. Process Des. Dev., 18, 607 (1979).

Borgwardt, R.H., and R.D. Harvey, Environ. Sci. Technol., 6, 350 (1972).

Borgwardt, R.H., and N.F. Roache, Ind. Eng. Chem. Process Des. Dev., 23, 742-748 (1984).

Borgwardt, R.H., N.F. Roache, and K.R. Bruce, Environ. Prog., 3, 129-135 (1984).

Bulewicz, E.M., S. Kandefer, and C. Jurys, J. Inst. Energy, 188 (1986).

Dennis, J.S., and A.N. Hayhurst, Inst. Chem. Eng. Symp. Ser., 87, 61 (1984).

Dennis, J.S., and A.N. Hayhurst, Chem. Eng. Sci., 42, 2361 (1987).

Davies, N.H., K.M. Laughlin, and A.N. Hayhurst, Twenty-Fifth Symposium (International) on Combustion, pp. 211-218, The Combustion Institute, Pittsburgh, PA, 1994.

Efthimiadis, E.A., and S.V. Sotirchos, Ind. Eng. Chem. Res., 31, 2311 (1992).

Grindley, T., S.S. Kim, E.E. Gorski, and G. Steinfeld, "Aspects of the Design of a Process Development Unit for High-Temperature Coal Gas Desulfurization," Technical Report, DOE/METC-85/6025, 1985.

Gullett, B.K., and K.R. Bruce, AIChE J., 33, 1719 (1987).

Hajaligol, M.R., J.P. Longwell, and A.F. Sarofim, Ind. Eng. Chem. Res., 27, 2203 (1988).

Hartman, M., and R.W. Coughlin, Ind. Eng. Chem., Process Dec. Dev., 13, 248 (1974).

Hartman, M., and R.W. Coughlin, AIChE J., 22, 490 (1976).

Hasler J.R. et al., "Testing of limestone samples from the TVA region as sulfur dioxide sorbents in atmospheric fluidized bed combustors," Technical Report, Institute for Mining and Mineral Research, Univ. of Kentucky, 1984.

Hoke, R.C. et al., "Studies of the pressurized fluidized-bed coal combustion process," Technical Report, EPA-600/7-77-107, September 1977.

Jansson, S.A., L.P. O'Connell, and J.E. Stantan, Proc. Int. Conf. Fluid. Bed Combust., 7, 1095 (1982).

Krishnan, S.V., Ph.D. Thesis, University of Rochester, 1993.

Krishnan, S.V., and S.V. Sotirchos, "On the Mechanism of $SO_2$ Removal by Limestones under Simulated PFBC Conditions," Can. J. Chem. Eng., 71, 244 (1993a).

Krishnan, S.V., and S.V. Sotirchos, "A Variable Diffusivity Shrinking-Core Model and Its Application to the Direct Sulfation of Limestones," Can. J. Chem. Eng., 71, 724 (1993b).

Krishnan, S.V., and S.V. Sotirchos, "Theoretical and Experimental Investigation of the Direct Sulfidation of Limestones," Ind. Eng. Chem. Res., 33, 1444 (1994).

Ljungstrom, E., and O. Lindqvist, Proc. Int. Conf. Fluid. Bed. Combust., 7, 465 (1982).

Murthy, K. S., J. E. Howes, and H. Nack, Environ. Sci. Technol., 13, 197 (1979).

Newby, R.A., N.H. Ulerich, and D.L. Keairns, Proc. Int. Conf. Fluid. Bed Combust., 6, 803 (1980).

Ruth, L.A., A.M. Squires, and R.A. Graff, Environ. Sci. Technol. 6, 1009-1014 (1972).

Simons, G.A., and A.R. Garman, AIChE J., 32, 1491 (1986).

Smith, D. et al., Proc. Int. Conf. Fluid. Bed Combust., 7, 439 (1982).

Snow, M. J. H., J. P. Longwell, and A. F. Sarofim, ' Ind. Eng. Chem. Res. 27, 268 (1988).

Sotirchos, S.V., and S. Zarkanitis, AIChE J., 38, 1536 (1992).

Stantan, J.E., S.N. Barker, R.V. Wardell, N.H. Ulerich, and D.L. Keairns, Proc. Int. Conf. Fluid. Bed Combust., 7, 1064 (1982).

Tullin, C., and E. Ljungstrom, Energy & Fuels, 3, 284 (1989).

Ulerich, N.H., R.A. Newby, W.G. Vaux, and D.L. Keairns, Proc. Int. Conf. Fluid. Bed Combust., 7, 121 (1982).

Ulerich, N.H, E.P. O'Neill, and D.L. Keairns, "The Influence of Limestone Calcination on the Utilization of the Sulfur-Sorbent in Atmospheric Pressure Fluid-Bed Combustors," EPRI ER-426, Final Report, 1977.

Van der Ham, A.G.J., A.M. Heesink, W. Prins, and W.P.M. van Swaaij, Ind. Eng. Chem. Res., 35, 1487-1495 (1996).

Van Houte, G., L. Rodrique, M. Genet, and B. Delmon, Environ. Sci. Technol., 15, 327 (1981).

Vogel, G.J. et al., Quarterly Report (January-March 1977), prepared for DOE, Argonne National Laboratory, 1977.

Wen, C.Y., and M. Ishida, Environ. Sci. Technol., 7, 703( 1973).

Yen, J.H., K. Li, and F.H. Rogan, Chem. Eng. Comm., 10, 35-60 (1981).

Yrjas, K.P., M.M. Huppa, and K. Iisa, Energy and Fuels, 10, 1189-1195 (1996).

Yu, H.C., Ph.D Thesis, University of Rochester, 1987.

Zarkanitis S., Ph.D. Thesis, University of Rochester, 1991.

Zarkanitis, S., and S.V. Sotirchos, AIChE J., 35, 821 (1989).

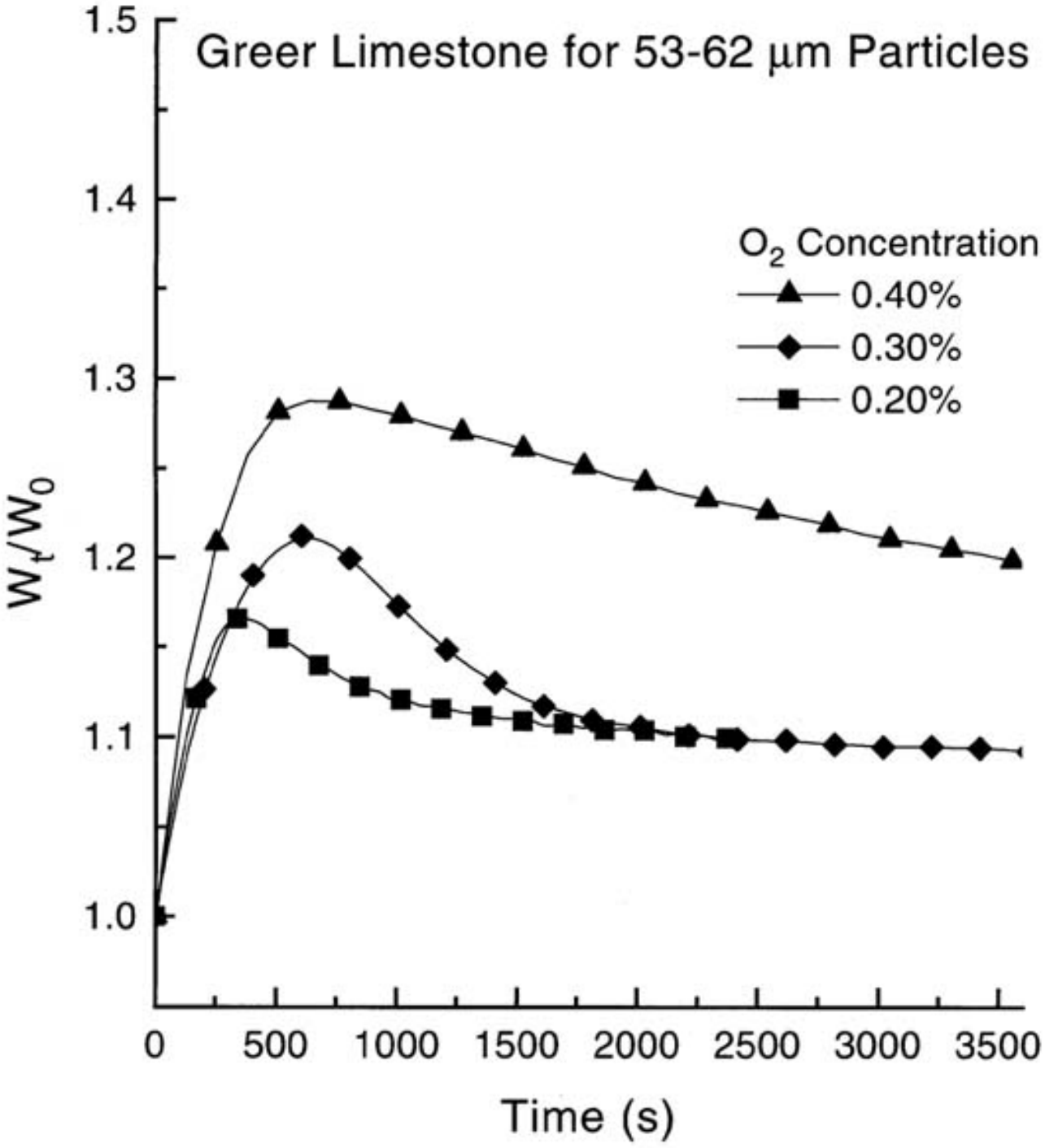


**Figure 1.** Weight change vs. time for Greer limestone 53-62 $\mu$m particles at 750 °C.

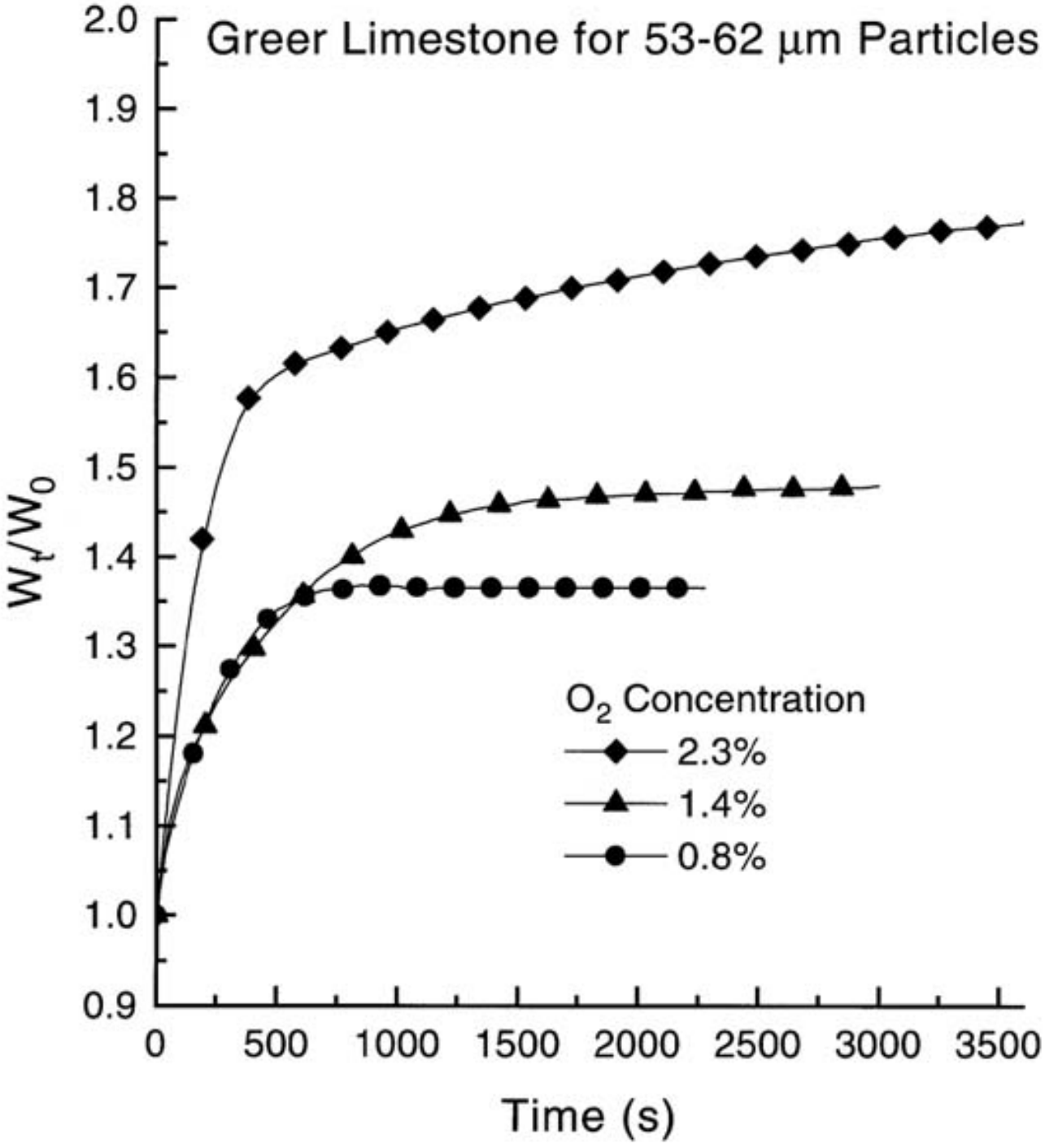


**Figure 2.** Weight change vs. time for Greer limestone 53-62 $\mu$m particles at 750 °C.

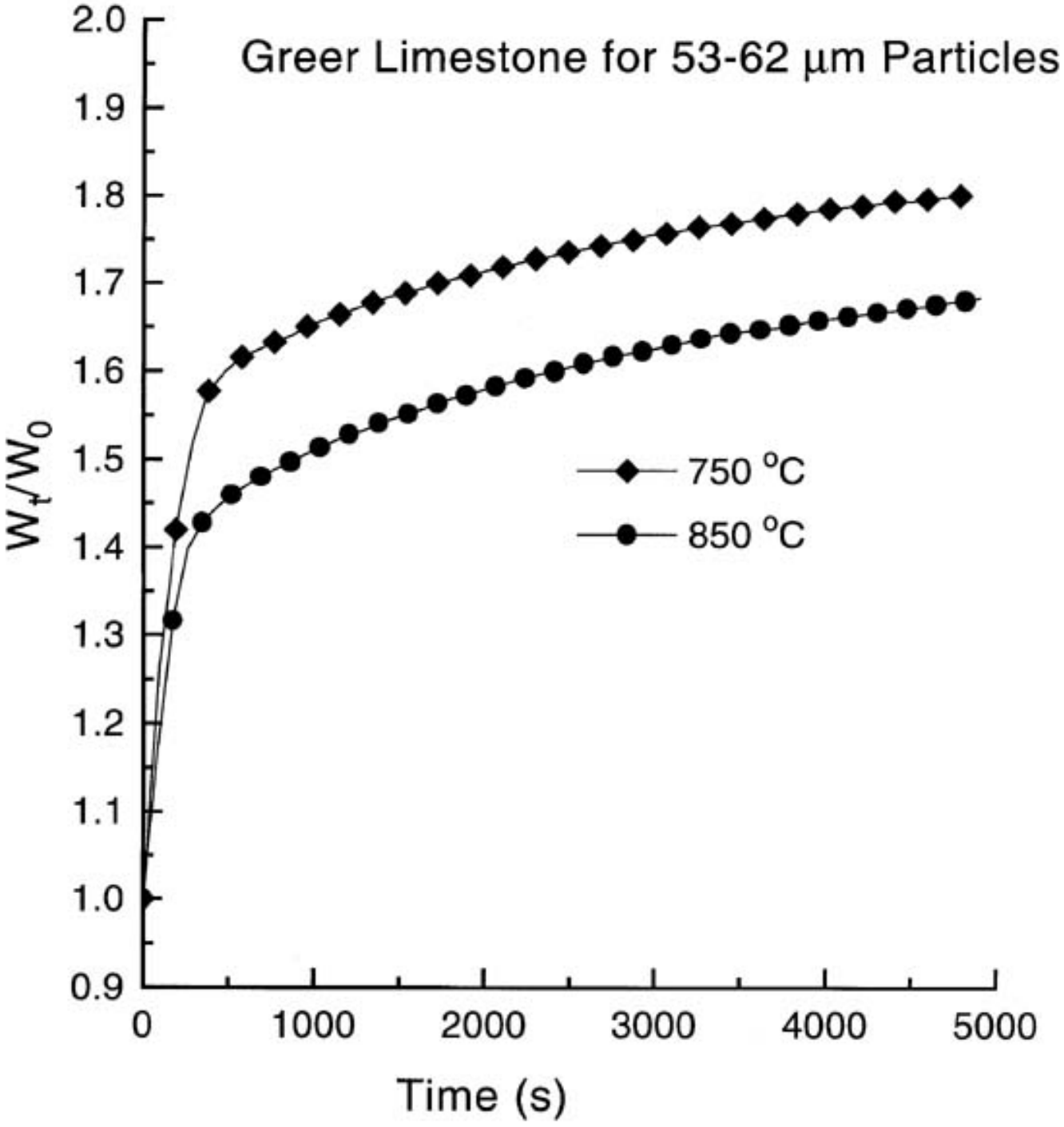


**Figure 3.** Weight change vs. time for Greer limestone 53-62 $\mu$m particles at 750 and 850 °C.

## APPENDIX

# A Stochastic Simulation Scheme for Studying Pore Volume Trapping in a Structure of Growing Particles

by

**Stratis V. Sotirchos***

Department of Chemical Engineering
University of Rochester
Rochester, New York 14627-1066

**and Manolis Tomadakis**

Chemical Engineering Program
College of Engineering
Florida Institute of Technology
Melbourne, Florida 32901-6975

*To whom correspondence should be addressed.

## ABSTRACT

A stochastic computational scheme is developed for investigating formation of trapped (isolated) pore volume in a structure of growing particles, with particle growth occurring only on surface elements exposed to the connected (accessible) part of the pore space. The simulation procedure combines a gradual increase of the particle size with a random walk scheme, the latter used to determine whether a randomly chosen point in the unit cell of the two-phase structure lies in the particle phase or in the connected or isolated part of the matrix phase. The formulated algorithm is applied to structures of freely overlapping, unidirectional cylinders, and results are obtained both for the volume fractions and the specific surface areas of the accessible and inaccessible parts of the pore phase. The trapped volume results are compared with those obtained for ordinary continuum percolation, that is, for uniformly growing particles.

# I. INTRODUCTION

Physical models that represent the solid phase of porous media as populations of solid objects are often used as a basis for transport or transport and reaction studies in porous media. By varying the size, orientation, and position distributions of these objects (grains or particles) a variety of physical models for porous media can be obtained. For many man-made porous materials, the representation of their solid phase by a 3-dimensional assemblage of solid objects offers a realistic representation of their structure. Examples of such porous media are materials prepared by compacting powders and the various fibrous materials that are employed as filtration media or reinforcing phase of composite materials.

There are many applications in which porous media participate in chemical reactions that lead to deposition of solid material on their internal surface (gas-solid interface). Deposition reactions almost always involve gaseous or liquid compounds transported to the reaction (deposition) interface through the pore space, and therefore, deposition can only take place on parts of the internal surface of the porous medium that can be accessed from the exterior, that is, parts that are boundaries to infinite subsets of the pore space. Typical examples of structure evolution driven by deposition reactions are offered by the process of chemical vapor infiltration for ceramic composite fabrication[1−3], where gaseous precursors are used to deposit carbon or ceramic materials on the internal surface of a porous medium (usually of fibrous structure) and the deactivation of catalysts through carbon deposition within their structure[4,5]. Structure evolution phenomena similar to those seen in deposition reactions are encountered in gas-solid reactions that form solid products that occupy more space than the solid reactants they replace. Such reactions are exemplified by several gas-solid reactions used in pollution control applications, such as the removal of hydrogen sulfide and sulfur dioxide from coal utilization gases using calcined limestones (i.e., porous calcium oxide)[6−8].

The evolution of the structure of a porous medium whose solid phase is represented as population of grains or particles can be followed by keeping the positions of the particles fixed and moving the points of their surface in the direction of the outward-pointing normal vector with the same velocity. In accordance with the preceding discussion, growth of particles can occur only on those parts of their surface that are boundaries to infinite regions

of the pore space. Since particle growth leads to diminishing porosity and interstitial distances in the pore space, areas of the pore space that are accessible at the outset of the process may be cut off from the infinite regions and become inaccessible. When particle growth reaches a critical level (the percolation threshold), the pore space ceases to percolate – it exists only as finite regions – and further deposition and structure evolution become impossible.

Uniform particle growth and formation of inaccessible pore space are schematically illustrated in Figure 1 for the case of a physical model consisting of disks on a plane or unidirectional cylinders in three dimensions. To point out the difference between the process characterized by uniform particle growth (ordinary percolation) and the growth process that requires transport of fluid precursors to the fluid-solid interface, particle growth is represented using two distinct layers. The layer that is indicated by the lighter gray color corresponds to particle growth that has occurred after the formation of the inaccessible region $I$, and therefore, its part that lies within $I$ cannot be formed through a deposition or gas-solid reaction process under physically realizable conditions. For obvious reasons, it is much easier to study the ordinary percolation process in which the particles are assumed to grow on all points of their surface, including those that bound inaccessible (trapped) regions of the pore space. Since the accessibility characteristics of the structure are not affected by whether the inaccessible (finite) regions of the pore space are allowed to shrink or not, the information that is extracted from the study of the ordinary percolation problem on the dependence of the accessible pore volume fraction and of its properties on particle growth is also applicable when pore volume trapping is taken into account. The variation of the accessible and inaccessible pore volume fraction and internal surface area during ordinary percolation can be employed – as it will be shown later – to determine the true inaccessible volume fraction, but a direct simulation scheme of the trapping process is required to determine other characteristics of the inaccessible areas, such as specific surface area and size distribution.

The formation of inaccessible (trapped) pore volume in porous media undergoing reactions that lead to diminishing porosity has been investigated only in the context of using a pore network or an abstract bond-site lattice to represent the porous medium.

A simulation scheme was employed to determine the connectivity characteristics of the accessible pore structure by Sahimi and Tsotsis[5], whereas Yortsos and Sharma[9], Yu and Sotirchos[10], and Sotirchos and Zarkanitis[7] determined them analytically from information for ordinary percolation by utilizing the observation that the evolution of the accessible pore, bond, or site clusters remains the same if entities are removed randomly not only from the accessible but from the inaccessible clusters as well. n equivalent observation for the problem we examine in the present study is – as we have already indicated in the previous paragraph – that the evolution of the accessible pore or matrix space with a variable describing the change of the size of the constitutive elements (grains) of the structure is the same as in the percolation process in which the grains are allowed to grow uniformly. Thus, it is not appropriate to describe the above processes as correlated processes, a term usually reserved for processes in which there are spatial correlations among the bonds of the lattice for discrete percolation problems or the particles (grains) for continuum correlation problems[11–13]. Another point that must be made is that the process of pore (bond) isolation or pore (matrix) volume trapping that characterizes these processes can also be encountered in correlated percolation problems. We therefore choose to describe the process we study as percolation with trapping, a term used by Dias and Wilkinson[14] to describe a similar situation that arises in an invasion percolation process involving two immiscible fluids on a lattice, where only the infinite clusters of the defender fluid are modified as the occupying fraction of the invader is increased.

A computational algorithm is formulated in the present study for studying pore volume trapping in a system of growing particles whose structure is modified through deposition on the surface of the particles involving species transported through the pore space to the reaction sites. It is based on a Monte Carlo simulation scheme that combines discrete (gradual) increase of the particle size with random walk computations. Points are placed randomly in a cubic unit cell of the particle structure and used as starting positions of random walkers that move through the matrix phase by suffering successive diffuse reflections on the surface of the particles. By employing a method first proposed by Burganos and Sotirchos[15], the trajectories of the random walkers are used to determine which of the randomly chosen points lie in the particle phase and in the connected and

isolated parts of the pore space at each step of particle growth. Further analysis of the trajectory data makes possible to determine the evolution of accessible, inaccessible, and total matrix volume fraction, average pore size, and surface area, with the particle size. It is also possible to find the Knudsen diffusion coefficient of gases in the pore space by using the information on the variation with time of the mean square displacement of the random walkers that travel in the accessible regions of the pore space. Results are presented on the application of the method to a random array of fully penetrable (freely overlapping) unidirectional cylinders. The computed trapped pore volume fraction at the percolation threshold is compared to that obtained from uniform particle growth computations.

## II. DESCRIPTION OF THE METHOD

We describe in this section the general aspects of the computational scheme that we have developed for studying correlated percolation in a system of growing particles. We also describe the derivation of an equation that may be used to follow the evolution of the accessible pore volume fraction during percolation with volume trapping using the results from the percolation process for uniform particle growth. Since the analysis we present applies to any two-phase composite medium in which one of the phases exists in the form of an assemblage of particles, the term matrix phase or matrix is employed when reference is made to the phase that surrounds the particle assemblage (i.e., the pore space in a porous medium).

### II.1. Determination of Matrix Connectivity from Random Walk Results

In the method formulated by Burganos and Sotirchos[15], random points are introduced in a representative unit cell of the two-phase medium and those that fall in the matrix phase are used as starting positions of random walkers. The trajectories of the random walkers are then employed to determine whether a starting point lies in the accessible (connected) or isolated part of the matrix. Each walker is assumed to move through the matrix phase of the two-phase medium by undergoing diffuse reflections (according to the cosine law) at the interface. Thus, its trajectory consists of straight segments that begin and end at the matrix-particle interface.

Walkers that remain confined in regions smaller than a threshold value as the time of

travel increases are assumed to travel in isolated (inaccessible) parts of the matrix phase. When all interfaces are oriented parallel to some direction – as it is the case with structures in which one of the phases consists of a population of unidirectional cylinders – accessibility is defined on planes perpendicular to that direction. Let $N$ be the total number of points chosen within the unit cell, $N^P$ the number of points that fall in the particle phase, $N^A$ the number of points that serve as starting points of trajectories that cover regions of space larger than the chosen threshold limit, and $N^I$ the number of points that yield trajectories confined within region smaller than that value. Since the points are selected randomly over the whole unit cell, the following relationships can be used to determine the volume fraction of the matrix phase, $\epsilon$, and its accessible and inaccessible parts, $\epsilon^A$ and $\epsilon^I$:

$$\epsilon = 1 - \frac{N_P}{N};\ \epsilon^A = \frac{N^A}{N};\ \epsilon^I = \frac{N^I}{N} \qquad (1a, b, c)$$

The specific surface area (per unit of total volume) of the interface that bounds one of the components of the structure (matrix phase, particle phase, inaccessible matrix phase, or accessible matrix phase) can be determined using the equation[16,17],

$$S = \frac{4\phi}{\bar{d}} \qquad (2)$$

where $\phi$ is the volume fraction and $\bar{d}$ the mean chord length of the component we are interested in. Since the cosine law is used to determine the direction of the path that a random walker follows after a collision with the particle-matrix interface, each path lies on a line of random orientation in space. As a result, the mean chord length of a certain region (connected or disconnected) is equal to the mean path of all random walkers that have travelled in the same region, each accomplishing the same travel distance. This quantity can be obtained directly from the results of the trajectory computations. For the total, accessible, and inaccessible specific surface areas of the matrix phase, $S$, $S^A$, and $S^I$, the general relationship of equation (2) yields the equations:

$$S = \frac{4\epsilon}{\bar{d}};\ S^A = \frac{4\epsilon^A}{\bar{d}^A};\ S^I = \frac{4\epsilon^I}{\bar{d}^I} \qquad (3a, b, c)$$

It should be noted that equations analogous to (1) and (3) also apply to each indi-

vidual fragment of the isolated (inaccessible) part of the matrix phase. Therefore, if one can identify all molecules that travel in the same fragment, those equations can be used to determine the volumes and surface areas of individual fragments and in this way construct fragment size and surface area distributions. Burganos and Sotirchos based the identification of fragments on the extremal coordinates of the trajectory of a random walker $(x_{\min}, x_{\max}, y_{\min}, y_{\max}, z_{\min}, z_{\max})$. Specifically, two or more walkers were considered to travel in the same fragment if the same extremal coordinates of their trajectories for large travel times did not differ by more than a small number that was of the order of the pore size used in the construction of the pore network.

### II.2. Algorithm for Following Matrix Volume Trapping

The application of the method begins with the construction of a unit cell of the two phase medium, usually of cubic shape. In the case of a structure of randomly overlapping particles, this is accomplished by simply introducing at random locations and according to the chosen size and shape distributions the particles that may wholly or partly lie in the cubic unit cell. By applying periodic boundary conditions in the construction of the unit cell – if the application of such conditions is possible – and arranging identical unit cells side by side, an infinitely large structure that spans the whole space and is statistically representative of the two-phase medium is obtained. If construction of periodic unit cells is not possible – as is the case with structures of infinitely long cylinders oriented randomly in two or three directions – an infinitely large structure can be obtained by filling the space with unit cells derived from the constructed unit cell so that all neighboring cells are mirror images of each other relative to their common face.

Once the construction of the unit cell is completed, the method proceeds with the generation of a sequence of derivative structures (daughter structures) of decreasing matrix volume fraction by enlarging uniformly all particles that make up the unit cell of the original structure. A schematic flow diagram of the procedure is given in Fig. 2. We use index 0 to represent the initial (mother) structure, $\mathcal{U}_0$, and indices $i = 1, 2, \ldots$ to represent the resulting daughter structures of uniformly grown particles, $\mathcal{U}_i$, in the order of decreasing matrix volume fraction. We introduce $N_0$ test molecules in the unit cell of

the mother structure and determine using the criteria described in the preceding section, the number of test molecules that fall in the particles $P_0$, in the connected part of the matrix phase $A_0$, and in the isolated part of the matrix phase, $I_0$. The points that are found to lie in the connected part of the matrix phase of the mother structure are then used as starting points of molecular trajectories in the first daughter structure, and the information extracted from these trajectories is used to determine the number of the $A_0$ points that fall in the connected part of the first daughter structure, $A_1$, the number of points that fall in its particle phase, $P_1$, and the number of points that fall in the isolated matrix phase, $I_1$. We continue with the $A_1$ points from the first daughter structure and use trajectory information from the second structure to partition their number into $A_2$, $P_2$, and $I_2$ parts. This process continues until we encounter a daughter structure, say $\mathcal{U}_N$, that does not show any connected matrix.

The derivative structures employed in the above described sequence of trajectory computations are obtained by letting all particles grow uniformly. As a result, they are not representative of the real structures, $\mathcal{R}_i$, that would be obtained if particle growth occurred by deposition of solid material transported into the structure from the outside, since in this case only the connected phase would be growing. The following three observations may be used to employ the $A_i$, $P_i$, and $I_i$ results to determine matrix phase and inaccessible volume information for the true derivative structures: i) Any point that lies in the accessible phase of the $i$th uniformly grown daughter structure, $\mathcal{U}_i$, would also lie in the accessible phase of the $i$th real daughter structure, $\mathcal{R}_i$ – since the accessible parts of grown and real daughter structures of the same generation uniformly are identical. ii) If a point lies in the solid phase of the mother structure, it will also belong to the solid phase of any real daughter structure – since the solid phase of the mother structure is a subset of that of the daughter structure. This also holds for any daughter structure and the derivative structures that result from it. iii) If a point lies in the isolated phase of $\mathcal{R}_i$ it will also lie in the isolated phase of any real structure with index greater than $i$ – since in real structures isolated regions do not change after they are formed.

Let $N_i^P$, $N_i^A$, and $N_i^I$ be the number of molecules from the initial number $N_0$ introduced in the unit cell of the mother structure that would have fallen in the particle

phase, accessible matrix phase, and inaccessible matrix phase, respectively, of the $i$th real daughter structure, $\mathcal{R}_i$. It follows from the above observations that $N_i^P$, $N_i^A$, and $N_i^I$ can be obtained from the following relationships

$$N_i^A = A_i;\ N_i^P = \sum_{j=0}^{i} P_j;\ N_i^I = \sum_{j=0}^{i} I_j \qquad (4a,b,c)$$

For the mother structure, we obviously have

$$N_0^A = A_0;\ N_0^P = P_0;\ N_0^I = I_0 \qquad (5a,b,c)$$

Since $A_{i-1} = A_i + P_i + I_i$, it follows that $N_i^A + N_i^P + N_i^I = N_0$ – as it should be the case.

With $N_i^A$, $N_i^P$, and $N_i^I$ known, equations (1) and (3) can be used to determine all structural properties of the $i$th real daughter structure. For the porosities, we have from equations (1)

$$\epsilon_i^A = \frac{N_i^A}{N_0};\quad \epsilon_i^I = \frac{N_i^I}{N_0};\quad \epsilon_i = \frac{N_0 - N_i^P}{N_0} \qquad (6a,b,c)$$

The mean path of the $N_i^A$ walkers for the $i$th set of trajectory computations is equal to the mean random chord of the accessible space, $\bar{d}_i^A$, and it can thus be used to determine the accessible surface area per unit volume. Similarly, the mean chord length of the inaccessible space is equal to the mean path of the $N_i^I$ molecules. It can be estimated using $I_0$ trajectories from the mother structure and $I_j$ $(j = 1, ..., i)$ for the daughter structures. From equations (3), we have

$$S_i = \frac{4\varepsilon_i}{\bar{d}_i};\ S_i^A = \frac{4\varepsilon_i^A}{\bar{d}_i^A};\ S_i^I = \frac{4\varepsilon_i^I}{\bar{d}_i^I} \qquad (7a,b,c)$$

The above computation scheme yields discrete approximations to the $\varepsilon^A$ vs. $\varepsilon$ or $\varepsilon^I$ vs. $\varepsilon$ curves that would be observed during densification of the porous medium through solid deposition on its accessible surface. The difference between the discrete approximation and the exact result can be reduced by decreasing the growth distance between successive structures or, equivalently, by increasing the number of daughter structures between the mother structure and the structure at the percolation threshold.

### II.3. Computation of Quantities for Uniform Particle Growth

With minimal additional effort, the results from the above computations can also be used to compute properties for the uniform particle structures. Let $I_j^i$ be the number of the $I_j$ isolated walkers found in the $j$th uniform structure that fall in the gas phase in the $i$th uniform structure $j < i$. These walkers can easily be identified by comparing their initial locations with the space occupied by the particles in the $i$th uniform structure. We do not have to examine the locations of all of the $I_j$ walkers in each of the subsequent structures since those isolated walkers that fall in the solid phase of the $i$th structure will also fall in the solid phase of all subsequent structures. The total number of walkers that fall in the inaccessible space in the $i$th uniform daughter structure is given by $(I_i + \sum_0^{i-1} I_j^i)$, the total number of walkers that fall in the inaccessible space is $A_i$, the same as in the real structure, and the total number of walkers that fall in the solid phase is $(\sum_0^i P_j + \sum_0^{i-1}(I_j - I_j^i))$. Let superscript $u$ denote quantities referring to the structures of uniformly grown particles or, equivalently, the percolation problem that is commonly considered. On the basis of the above observations, we have:

$$\varepsilon_i^{uA} = \frac{A_i}{N_0} = \varepsilon_i^A \tag{8a}$$

$$\varepsilon_i^{uI} = \frac{I_i + \sum_0^{i-1} I_j^i}{N_0} < \varepsilon_i^I \tag{8b}$$

$$\varepsilon_i^u = \frac{N_0 - (\sum_0^i P_j + \sum_0^{i-1}(I_j - I_j^i))}{N_0} = \varepsilon_I^A + \varepsilon_i^{uI} < \varepsilon_i \tag{8c}$$

The internal surface areas of the uniform particle structures can be computed using equations analogous to those (equations (7)) for the real structures. The accessible surface area per unit volume of the uniform particle structures is the same as that of the real structures. To compute $\bar{d}_i^u$ and $\bar{d}_i^{uI}$, we need information on the trajectories of the $(\sum_0^{i-1} I_j^i)$ walkers that travel in the inaccessible space of $i$th structure, and which have become isolated in earlier daughter structures. Since we know that these molecules are isolated, we only have to let them travel for as much time (or distance) as needed to obtain a representative sample of random chords.

### II.4. Prediction of Trapped Volume Fraction from Uniform Growth Results

The uniform particle structure results can be used to predict the relationship between $\varepsilon^u$ and $\varepsilon$ and – since $\varepsilon^{uA}$ and $\varepsilon^A$ are equal – between $\varepsilon^A$ and $\varepsilon$. When the particles are assumed to grow uniformly, the inaccessible regions decrease in size, and this makes the difference between $\varepsilon$ and $\varepsilon^u$ progressively larger. As the particle growth variable changes from $q$ to $q + dq$, the change in the porosity of the inaccessible regions of the uniform structures is equal to $S^{uI}dq$. Since the difference in $\varepsilon$ and $\varepsilon^u$ is only due to the change in the size of the inaccessible regions, we must have

$$d(\varepsilon - \varepsilon^u) = S^{uI}dq \tag{9}$$

Integrating this equation between 0 and $q$ using that $\varepsilon|_{q=0} = \varepsilon^u|_{q=0} = \varepsilon_0$ gives

$$\varepsilon = \varepsilon^u + \int_0^q S^{uI}dq' \tag{10}$$

This equation is a rigorous result and can be used to find $\varepsilon$ as a function of $\varepsilon^u$, and vice versa, for any particle structure provided that the variation of $S^{uI}$ with $q$ is known. Since the accessible pore space is the same in uniform and real structures, $\varepsilon^A(\varepsilon)$ can be found as $\varepsilon^{uA}(\varepsilon^u(\varepsilon))$. Equation (10) could also be derived by using the relationships

$$d\varepsilon^u = -(S^{uI} + S^{uA})dq$$

$$d\varepsilon = -S^{uA}dq = -S^A dq$$

or equivalently,

$$\varepsilon^u = \varepsilon_0 - \int_0^q (S^{uI} + S^{uA})dq'$$

$$\varepsilon = \varepsilon_0 - \int_0^q S^{uA}dq'$$

The properties of the uniform particle structures can be computed using the general method of Section II.1 or in conjunction with the percolation with volume trapping computations, as described in Section II.3. Suppose that there are $n - 1$ uniform particle

structures between the starting (mother) structure and the percolation threshold. Using the trapezoidal rule to evaluate the integral in equation (10), we get

$$\varepsilon_i = \varepsilon_i^u + \sum_1^i \frac{(S_j^{uI} + S_{j-1}^{uI})}{2}(q_j - q_{j-1}) \tag{11}$$

For the percolation threshold, i.e., the porosity of the $n$th daughter structure, this equation gives

$$\varepsilon_p = \varepsilon_p^u + \sum_1^n \frac{(S_j^{uI} + S_{j-1}^{uI})}{2}(q_j - q_{j-1}) \tag{12}$$

The advantage of using equation (11) to find the total, accessible, and inaccessible porosities of the volume trapping percolation problem is that only information for the uniformly grown grain structures is needed, that is, the volume trapping algorithm does not have to be employed. Since an integral formula is employed, relatively accurate results can be obtained with only a few daughter structures. However, the volume trapping algorithm has the advantage that it can provide information for all properties of the volume trapping percolation problem and not only for the porosities (volume fractions).

Let $\alpha$ be the ratio of the mean random chord of the total pore space, $\bar{d}^u$, to the mean random chord of the inaccessible space, $\bar{d}^{uI}$. Using equation (3), we can write for $S^{uI}$

$$S^{uI} = \alpha S^u \frac{\varepsilon^{uI}}{\varepsilon^u} = \alpha S^u (1 - \frac{\varepsilon^{uA}}{\varepsilon^u}) \tag{13}$$

Introducing this equation in (9) and using $d\varepsilon^u = S^u dq$ to change the variable of integration from $q$ to $\varepsilon^u$, we get

$$\varepsilon = \varepsilon^u + \int_{\varepsilon^u}^{\varepsilon_0} \alpha(1 - \frac{\varepsilon^{uA}}{\varepsilon'})d\varepsilon' \tag{14}$$

where $\varepsilon_0$ is the common value of $\varepsilon$ and $\varepsilon^u$ for growth zero. For $\alpha$ being approximately constant, equation (14) can be used to derive an approximate expression for $\varepsilon(\varepsilon^u)$ that involves only $\varepsilon^{uA}(\varepsilon^u)$. For example, if the mean random chord lengths of the total pore (matrix) space and of the inaccessible pore space of the uniform structures are assumed to be approximately equal to each other, i.e., $\alpha = 1$, we get

$$\varepsilon = \varepsilon_0 - \int_{\varepsilon^u}^{\varepsilon_0} \frac{\varepsilon^{uA}(\varepsilon')}{\varepsilon'} d\varepsilon' \tag{15}$$

In their study of percolation during uniform growth of structures of randomly overlapping unidirectional cylinders, Burganos and Sotirchos found that that $\bar{d}^{uI}/\bar{d}^{u}$ was significantly larger than 1. Therefore, equation (15) is expected to underestimate $\varepsilon$ for such structures.

## III. APPLICATION

We applied the formulated algorithm to a porous medium whose structure can be represented by a population of randomly overlapping, unidirectional cylinders. A unit cell for this structure was constructed by positioning randomly the traces of the axes of the cylinders on one of the faces of a cube. In order to obtain a periodic unit cell spanning the whole space, periodic boundary conditions were employed[18]. In an infinitely large structure, the porosity (matrix volume fraction) is given by[19,20]

$$\varepsilon^u = \exp(-\pi \ell r^2) \tag{16}$$

where $\ell$ is the cylinder density, i.e., the total length of cylinder axes per unit volume or the number of traces of axes on the cubic face, and $r$ is the radius of the cylinders. We have used superscript $u$ on $\varepsilon$ because the structure it refers to is composed of perfect cylinders, i.e., uniformly grown particles. For finite realizations (samples) of the porous medium, equation (16) gives the mean value of porosity for a large number of realizations. The porosity of the finite samples we constructed for computations was determined by introducing $10^7$ points randomly in the cubic cell and computing the fraction that fell in the matrix phase.

Past studies[15,18,21] showed that the percolation threshold of a structure of randomly overlapping, unidirectional cylinders, $\varepsilon_p^u$, is equal to about 0.325. Like the porosity given by equation (16), this value gives the percolation threshold of an infinite structure or the mean value of the percolation threshold of a large number of finite realizations. The results we present and discuss here were obtained using sample structures having percolation thresholds very close to the mean value. We used a cluster identification scheme[15,18] to determine the percolation thresholds of the unit cells we constructed, and only structures

that had percolation thresholds for uniform cylinder growth between 0.315 and 0.335 were employed for random walk computations. To identify such samples we started from dense cylinder structures having porosity (matrix volume fraction) much lower than the mean percolation threshold. This was done because as the cylinder size is increased, cylinders that initially lie wholly within the cell boundaries start to intersect the boundaries, and it thus becomes necessary to introduce more cylinders to maintain the periodicity of the unit cell.

The cluster identification scheme proceeds as follows: A sequence of derivative structures is constructed by reducing the cylinder radius by a certain amount $\Delta r$, and for each of them, a search is made for clusters of cylinders spanning the unit cell. When a structure with permeable matrix (that is, a structure for which no spanning clusters can be found) is encountered, the percolation threshold radius of the structure is approximated as the mean of the values that yield successive impermeable and permeable structures. To obtain a more accurate estimate of the percolation radius, we repeat the above procedure starting from the last impermeable structure with an order of magnitude smaller step, and we can continue doing this until the desired accuracy is obtained. The percolation threshold porosity is then determined as the probability to find a random point in the pore space. It should be noted that in order to guarantee that a cell-spanning cluster would extend to infinity, a cluster is considered to span the unit cell only when it includes at least one boundary cylinder and its periodic image on the opposite phase of the cylinder.

To apply the algorithm of Section II.2 to study correlated percolation in the unidirectional random cylinder structure, the radius of the cylinders is reduced until a structure possessing no inaccessible pore space is obtained. A significant amount of inaccessible pore space exists in that structure only close to the percolation threshold[15,18], and for porosities ($\varepsilon^u$) above 0.4 it turns out that almost all pore space is accessible. Using equation (16), it is found that about 10% reduction in the cylinder radius is required to bring the porosity from its percolation threshold value (0.325) to 0.4. A random walker is assumed to travel in an inaccessible fragment of the pore space if the maximal $x$ or $y$ coordinates of its trajectory, within the allotted travel time, do not exceed the corresponding minimal values by more than the side of the unit cell. In the $z$ direction (i.e. parallel to the cylinders),

the structure is connected at all porosities. Burganos and Sotirchos considered in their study that molecules travelled in inaccessible fragments if they did not visit, again within the allotted time, cells that did not border the cell from which they started their travel. Computations using this last criterion were also carried out, but no significant differences from the results computed using the first criterion were obtained.

For insufficiently long travel times, or equivalently distances, the results are strongly depended on travel time or distance. If the time of travel is not large enough, molecules travelling in connected areas with small necks may wrongly be classified as travelling in inaccessible fragments. Figure 3 presents the variation of the fraction of random walkers that are found to travel in the accessible void space with the travel distance for an array of fully penetrable unidirectional cylinders with $r/r_p = 0.97$. The fraction is taken relative to the number of walkers that were determined to travel in the accessible void (matrix) space of the structure with $r/r_p = 0.96$. The results of Figure 3 indicate that about 3% of the walkers travel in finite size subsets of the matrix phase; therefore, about 3% of the matrix phase of the daughter structure with $r/r_p = 0.97$ that is contained in the accessible matrix phase of the structure with $r/r_p = 0.96$ is inaccessible. However, travel distances greater than about $5 \cdot 10^5$ cylinder radii had to be employed to obtain this result. Random walkers that were found to travel in the accessible pore space accomplished an average distance of 107,000 radii by the time they attained net displacement equal to one cell side.

The expression for the first passage probability of molecules diffusing in the accessible void space of the molecules through molecule-wall collisions may be employed to understand better the results of Figure 3. The first passage probability of a diffusion process gives the probability that a random walker reaches a given distance from the origin for the first time within the time interval $(t,t + dt)$. Since a molecule is considered to travel in the accessible part of the pore space if the difference between the minimal and maximal coordinates of its trajectory in the $x$ or $y$ direction (that is, on the plane normal to the direction of the cylinders) is greater than one unit cell side, it may be argued that in the absence of inaccessible pore space, the ordinate in Figure 3 approximately corresponds to the probability that a random walker is displaced from the origin by a distance greater than half of the unit cell side on the $(x, y)$ plane for travel distance smaller than the value

of the abscissa. In other words, the ordinate in Figure 3 approximately represents the first passage probability for time less than that corresponding to the travel distance of the abscissa through a cylindrical boundary placed parallel to the cylinders and located at a distance equal to half of the unit cell side. For isotropic transport in two dimensions – as it is the case on the plane normal to the cylinders – it can be shown that the first passage probability for displacement distance $b$ is given by[22,23]

$$P_b(t) = 1 - \sum_{i=1}^{\infty} \frac{2}{j_i J_1(j_i)} e^{-j_i^2 D_e t/b^2} \tag{17}$$

where $J_1$ is the first order Bessel function of the first kind, $j_i$ is the $i$th zero of the zero order Bessel function of the first kind ($J_0$), and $D_e$ is the effective diffusion coefficient through the accessible void (matrix space) on the $(x, y)$ plane. The time that appears in equation (17) is for travel on the $(x, y)$ plane only. It is proportional to the travel distance of Figure 3, and therefore, equation (17) also applies in transport in three dimensions for first passage through a cylindrical enclosure.

Equation (17) states that the travel time required for a certain fraction of the random walkers that travel in the accessible part of the matrix space to reach a boundary located at a given distance from the origin of their travel is inversely proportional to their effective diffusivity. The effective diffusivity in the accessible matrix phase decreases as grain growth occurs and the porosity is decreased, becoming exactly zero at the percolation threshold. For this reason, the minimum travel distance that is needed to obtain an accurate count of the molecules that travel in inaccessible fragments of the matrix space becomes progressively larger as the radius of the cylinders is increased, diverging to infinity at the percolation threshold. By comparing the transmitted fraction of molecules through the cylindrical enclosure that is obtained from the simulations with that predicted by equation (17), it is possible to obtain estimates both of the effective diffusivity in the accessible part of the matrix phase and of the number of random walkers that travel in the inaccessible part of the matrix. The effective diffusivity estimate can subsequently be employed in equation (17) to determine the minimum travel time that is needed to obtain an accurate count of the random walkers that travel in the accessible part of the matrix.

Figure 4 shows how the error in the computation of the percolation threshold of the real structures (with volume trapping accounted for) with the number of steps from the mother structure ($r/r_p = 0.7325$ or $\epsilon^u \approx 0.55$) to the structure at the percolation threshold for two different realizations. For one step only, the predicted percolation threshold is equal to that found for uniformly grown structures. Since the percolation threshold of the real structures is close to that of the uniformly evolved structures, relatively good accuracy in its estimation is obtained even with a few structures. About 99% accuracy can be achieved using 10-15 discretization steps, but almost 100 steps are needed for an accuracy of 99.5%. The two realizations that were used to obtain the results of Figure 4 were among those that gave the largest difference between the percolation threshold for uniform grain (cylinder) growth and that with volume trapping taken into account.

Table I gives average values of total porosity, both for real and uniformly grown structures ($\varepsilon$ and $e^u$), and accessible porosity computed for eight realizations of a structure of unidirectional, randomly overlapping cylinders for a initial (mother) structure at $r/r_p = 0.7325$ and 10 derivative (daughter) structures, including that at the percolation threshold ($r/r_p = 1.0$). The number of cylinders in the unit cell ranged from 220 to 250, and 2500 starting points of random walkers were employed. The results of Table I show that the difference between the porosity of uniformly grown structures and that of real structures is very small. The average values of porosity at the percolation threshold for the eight structures of Table I was found to be 0.3275 for uniformly grown structures and 0.3347 for real structures. This result is in very good agreement with those obtained by Sahimi and Tsotsis[5], Yortsos and Sharma[9], Yu and Sotirchos[10], and Sotirchos and Zarkanitis[7] for the connectivity characteristics of pore networks in gas-solid reaction processes involving diminishing pore size, where only pores that belong to accessible (infinite clusters) can be plugged. For example, the computations of Sahimi and Tsotsis[5] for a showed that the percolation threshold, expressed in terms of the number fraction of unplugged pores (open bonds) of the network changes from 0.249 for the random percolation process to 0.255 for the real process in which inaccessible pores cannot undergo size change.

The existence of a small difference between the percolation thresholds of uniformly grown and real pore structures was postulated by us in past publications[18,21,24] on the

basis of the observation – as it is also seen from the results of Table I – that formation of significant amount of inaccessible pore space occurs in a very narrow range of pore space in the vicinity of the percolation threshold. The same observation led Ofori and Sotirchos[3], to assume when they modelled the process of chemical vapor infiltration for fabrication of ceramic matrix composites in uni-, bi-, or tridirectional random fiber structures (i.e., with fibers positioned in space parallel to a line (as in the application considered in the present study), parallel to a plane, or without preferred orientation) that formation of inaccessible pore space occurred right at the percolation threshold, which they set equal to that found for uniformly grown structures by Burganos and Sotirchos[15].

Figure 5 presents the evolution of the computed values of mean intercept length of the accessible, inaccessible, and total matrix phase with the cylinder radius, whereas the values of surface area that are determined using these results and the porosity values in equations (7) are shown in Figure 6. The theoretically predicted mean intercept length for uniformly grown arrays of fully penetrable (freely overlapping), unidirectional cylinders is also plotted in Figure 5. It is given by[20] $\bar{d}^u = 2/(\pi \ell r))$. It is seen from the results of Figure 5 that the dimensionless mean intercept length with volume trapping accounted for is slightly larger than that for uniformly grown structures. Since the internal surface area is for a given porosity, inversely proportional to the mean intercept length, the opposite observation holds for the dimensionless internal surface area values in Figure 7. The mean intercept length of the inaccessible matrix fragments is by a factor of about four smaller than that of the accessible matrix space, which implies that the inaccessible regions have, per unit of volume, surface areas larger by that factor than the accessible matrix. Both the accessible and total matrix mean intercept lengths decrease as the cylinder diameter increases, whereas that for the inaccessible (isolated) matrix increases. The surface areas change in the same way as the mean intercepts lengths and not in the opposite way, as expected from equations (7), because they are affected more by the change in the volume fractions. The volume of the inaccessible matrix fractions is obviously larger when volume trapping is accounted for, i.e., in the real structures, and this is the reason for which the real structures have larger surface areas.

At the percolation threshold, $r/r_p = 1.0$, all matrix space becomes inaccessible, and

the mean intercept length and surface area of the isolated matrix space become equal to the total matrix values. As we have already pointed out in the discussion of Table I, formation of a significant amount of pore space takes place in an very narrow region of values of cylinder radius or matrix volume fraction next to the percolation threshold. As a result, the mean intercept length of the isolated matrix space remains much smaller than that of the total matrix space even for values of dimensionless cylinder radius as high as 0.99. An analogous observation was made in past studies of the percolation behavior, for uniform fiber growth, of structures of multidirectional, randomly overlapping fibers (placed in space parallel to a plane or without any preferred orientation) and unidirectional (parallel), partially overlapping fibers[18,24]. In view of the results of Table I and of Figure 5 and 6, it is expected that the total matrix fraction, and hence, the percolation threshold, of these structures will not be affected significantly when volume trapping is taken into account. We tested this hypothesis by assuming that $\bar{d}^u/\bar{d}^{uI}$ for these structures had approximately the same average value as $\bar{d}/\bar{d}^I$ for parallel, unidirectional fibers (Figure 5) and using equation (14) to determine the total matrix volume fraction (porosity) with volume trapping using the $\varepsilon^{uA}$ vs. $\varepsilon^u$ from our previous studies. The obtained results showed that the inaccessible and total matrix volume fraction increase only slightly when occurrence of volume trapping is allowed for.

## IV. SUMMARY AND CONCLUSIONS

A stochastic simulation scheme was formulated for studying matrix volume trapping in structures of growing particles, where growth can occur only on surfaces that serve as boundaries of infinite (accessible) subsets of the matrix phase. The following steps are involved in the method: i) a unit cell is constructed for the starting (mother) structure, and the mother structure is used as basis for the construction of a number of derivative (daughter) structures of uniformly grown particles; ii) a number of points is selected randomly within the unit cell, and these points are used as starting points of random walkers that travel in the matrix space (outside the particles) by suffering diffuse reflections (according to the cosine law) on the particle surfaces; iii) such computations are carried out both for the initial and the derivative structures, and the information that is extracted from

these computations is employed to determine, for each uniformly grown structure, which of the randomly selected points in the two-phase medium lie in the particle phase, the accessible part of the matrix, or its inaccessible part; iv) the same determination is made for the real particle structures (that is, with matrix volume trapping accounted for) using a method developed in this study, and this information is further employed to estimate matrix volume fractions, mean intercept lengths, surface areas, and volume and surface area distributions of matrix phase fragments. In addition, we develop a formula that allows us to determine the variation of the inaccessible matrix volume of the real structures with the extent of particle growth from the variation of the surface areas and volume fractions of the inaccessible and accessible parts of the uniformly grown structures. The obtained results for the real structures are approximate, converging to the exact results as the steps between successive structures approach zero.

The method was applied to structures of randomly overlapping (fully penetrable), unidirectional cylinders. The comparison of the results for real and uniformly grown structures showed that the inaccessible and total matrix volume fractions increase by relatively small amounts when formation of trapped matrix (pore) space is taken into account. Since the inaccessible matrix fragments tend to have much larger surface area per unit volume than the accessible matrix space (by about a factor of 4 at the onset of formation of inaccessible matrix space starts), the total surface area of real structures is slightly larger than that of uniformly grown structures of the same particle size. It is believed that the reason for the existence of small differences between real (with volume trapping accounted for) and uniformly grown structures is that formation of inaccessible matrix space occurs at a significant rate only close to the percolation threshold. In past studies, this was also observed to be the case for structures of multidirectional, randomly overlapping fibers or unidirectional, partially overlapping fibers. It is thus expected that real and uniformly grown structures will exhibit small differences for these cases as well. This is a very important result for since it implies that the information that is available in the literature on the percolation behavior of the above fibrous media for uniform fiber growth can also be employed, without leading to significant errors for practical purposes, for the physically meaningful case where the fibers grow only on their accessible surfaces.

## ACKNOWLEDGMENTS

This work was supported by a grant from the U.S. Department of Energy.

## LITERATURE CITED

[1] R. Naslain, in *Ceramic matrix Composites*, R. Warren, Ed., Chapter 8, Chapman and Hall, Glasgow, 1992.

[2] T.M. Besmann, B.W. Sheldon, R.A. Lowden, and D.P. Stinton, Science, 253, 1104 (1991).

[3] J.Y. Ofori and S.V. Sotirchos, J. Electrochem. Soc., 143, 1962 (1996).

[4] B. Delmont and G.F. Froment, Eds., *Catalyst Deactivation* Elsevier, Amsterdam, 1980.

[5] M. Sahimi and T.T. Tsotsis, J. Catal., 96, 552 (1985).

[6] E.A. Efthimiadis and S.V. Sotirchos, Ind. Eng. Chem. Res., 31, 2311 (1992).

[7] S.V. Sotirchos and S. Zarkanitis, Chem. Eng. Sci., 48, 1487 (1993).

[8] A.B.M. Heesink and W.P.M. van Swaaij, Chem. Eng. Sci., 50, 2983 (1996).

[9] Y.C. Yortsos and M. Sharma, AIChE J., 32, 46(1986).

[10] H.C. Yu and S.V. Sotirchos, AIChE J., 33, 382 (1987).

[11] J.A. Given, J. Chem. Phys., 90, 5068 (1989).

[12] A.K. Sen and S. Torquato, J. Chem. Phys., 89, 3799 (1988).

[13] D. Stauffer, *Introduction to percolation theory*, Taylor and Francis, London and Philadelphia, 1985.

[14] M. Dias and Wilkinson, J. Phys. A: Math. Gen., 19, 3131 (1986).

[15] V.N. Burganos and S.V. Sotirchos, Chem. Eng. Commun., 85, 95 (1989).

[16] E.E. Underwood, *Quantitative Stereology*, Addison-Wesley, Reading, MA, 1970.

[17] A.M. Kellerer, Rad. Res., 47, 359 (1971).

[18] M.M. Tomadakis and S.V. Sotirchos, AIChE J., 37, 74 (1991).

[19] G.R. Gavalas, AIChE J., 26, 577 (1980).

[20] S.V. Sotirchos, Chem. Eng. Sci., 42, 1262 (1987).

[21] M.M. Tomadakis and S.V. Sotirchos, AIChE J., 37, 1175 (1991).

[22] L. Pontryagin, A. Andronow, and A. Witt, Zh. Eksp. Teor. Fiz., 3, 172 (1933).

[23] S. Lifson and J.L. Jackson, J. Chem. Phys., 36, 2410 (1962).

[24] M.M. Tomadakis and S.V. Sotirchos, J. Chem. Phys., 99, 9820 (1993).

Table I. Evolution of the porosity of uniformly grown structures, the porosity of real structures, and the accessible porosity with the cylinder size.

| $r/r_p$ | $\varepsilon$ | $\varepsilon^u$ | $\varepsilon^A$ |
|---|---|---|---|
| 0.7325 | 0.5489 | 0.5489 | 0.5489 |
| 0.75 | 0.5359 | 0.5358 | 0.5342 |
| 0.80 | 0.4926 | 0.4918 | 0.4899 |
| 0.85 | 0.4473 | 0.4459 | 0.4440 |
| 0.90 | 0.4035 | 0.4013 | 0.3980 |
| 0.95 | 0.3668 | 0.3636 | 0.3521 |
| 0.96 | 0.3607 | 0.3564 | 0.3450 |
| 0.97 | 0.3535 | 0.3483 | 0.3340 |
| 0.98 | 0.3465 | 0.3408 | 0.3229 |
| 0.99 | 0.3373 | 0.3311 | 0.3128 |
| 1.00 | 0.3346 | 0.3275 | 0. |

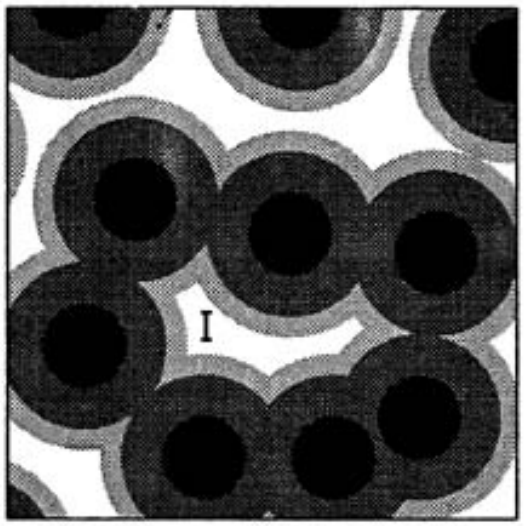


Figure 1. Schematic representation in two dimensions of particle growth under conditions leading to matrix volume trapping.

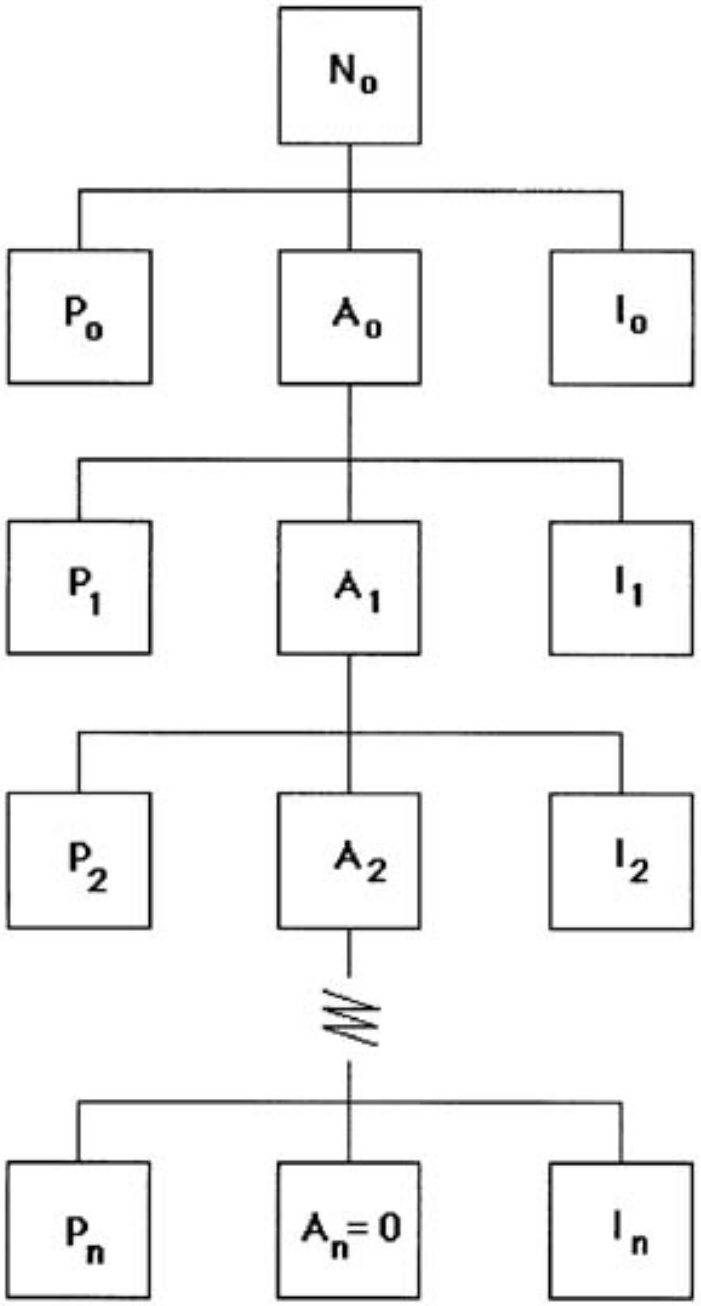


Figure 2. Flow diagram of the successive classification of the starting points of random walkers as lying in the particles, the accessible part of the matrix, or the inaccessible part of the matrix.

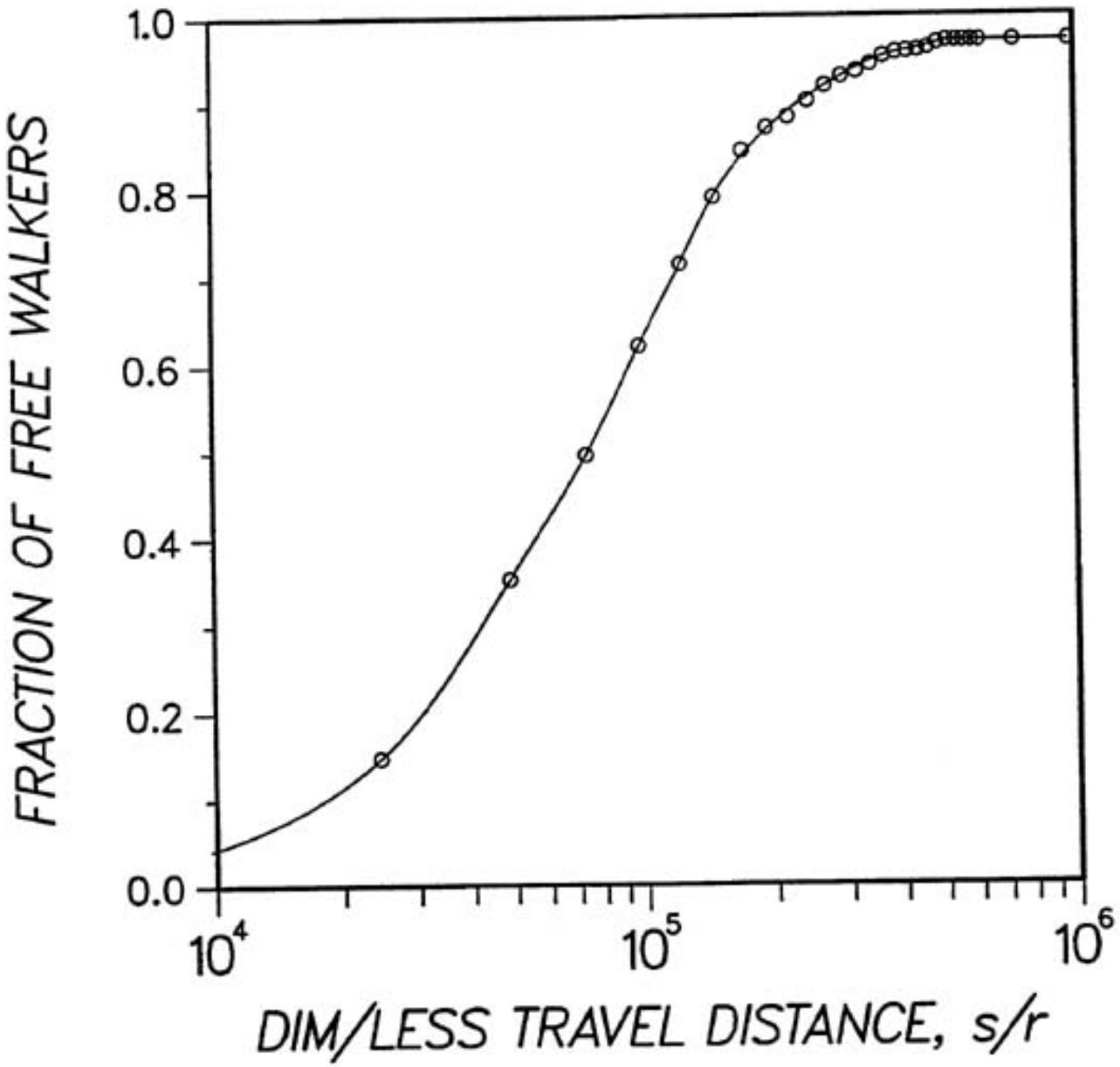


Figure 3. Variation of the fraction of random walkers determined to travel in the accessible matrix phase with the travel distance for a structure with $r/r_p = 0.97$. All starting points of random walkers were determined to lie in the accessible matrix of the structure with $r/r_p = 0.96$.

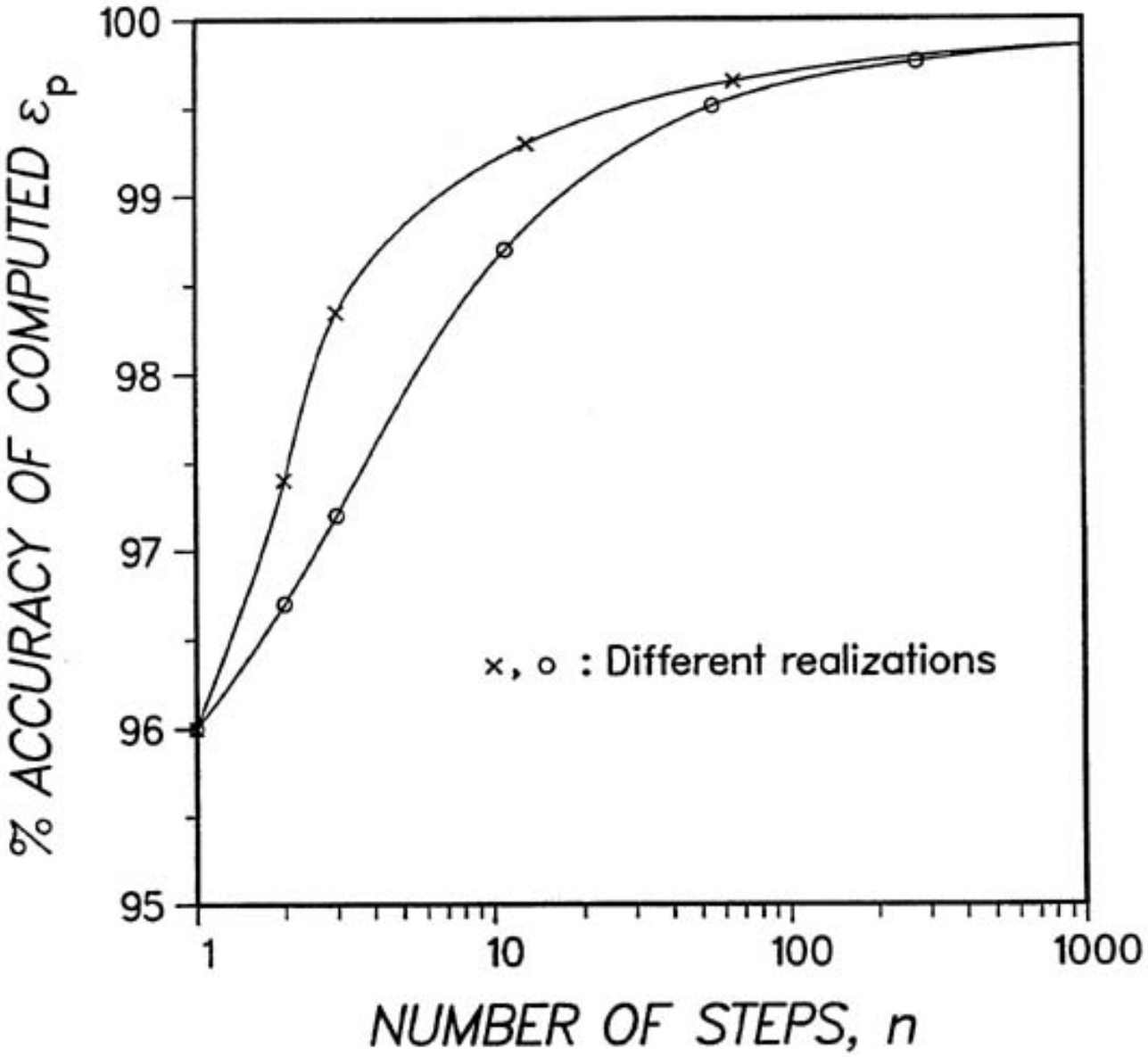


Figure 4. Evolution of the accuracy in the computed percolation threshold with the number of derivative (daughter) structures from $r/r_p = 0.7325$ to the percolation threshold in a structure of randomly overlapping (fully penetrable), unidirectional cylinders.

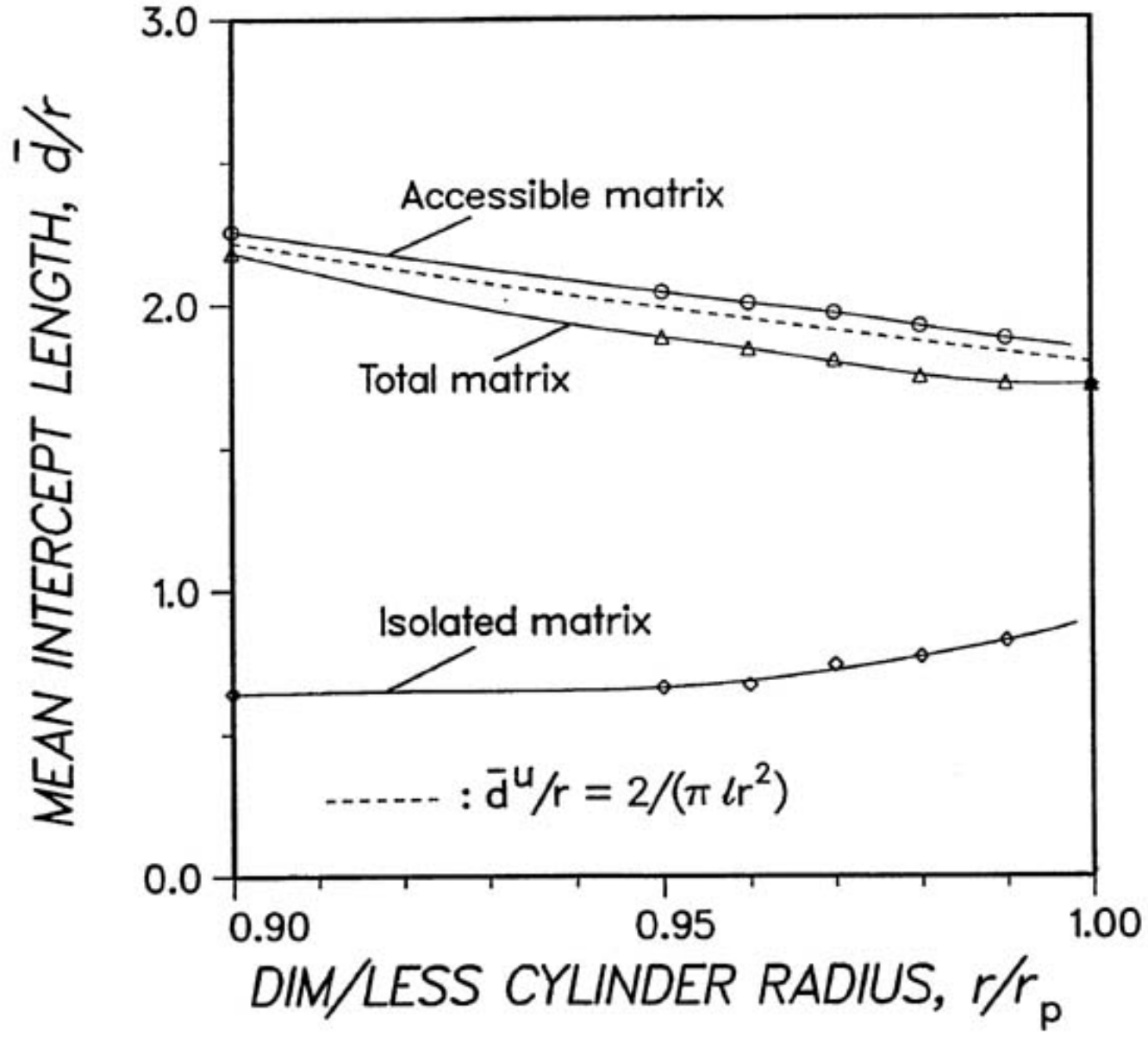


Figure 5. Variation of the dimensionless mean intercept length with the particle growth in random arrays of fully penetrable, unidirectional cylinders. The dashed curve gives the mean intercept length of the total matrix space for uniform particle growth.

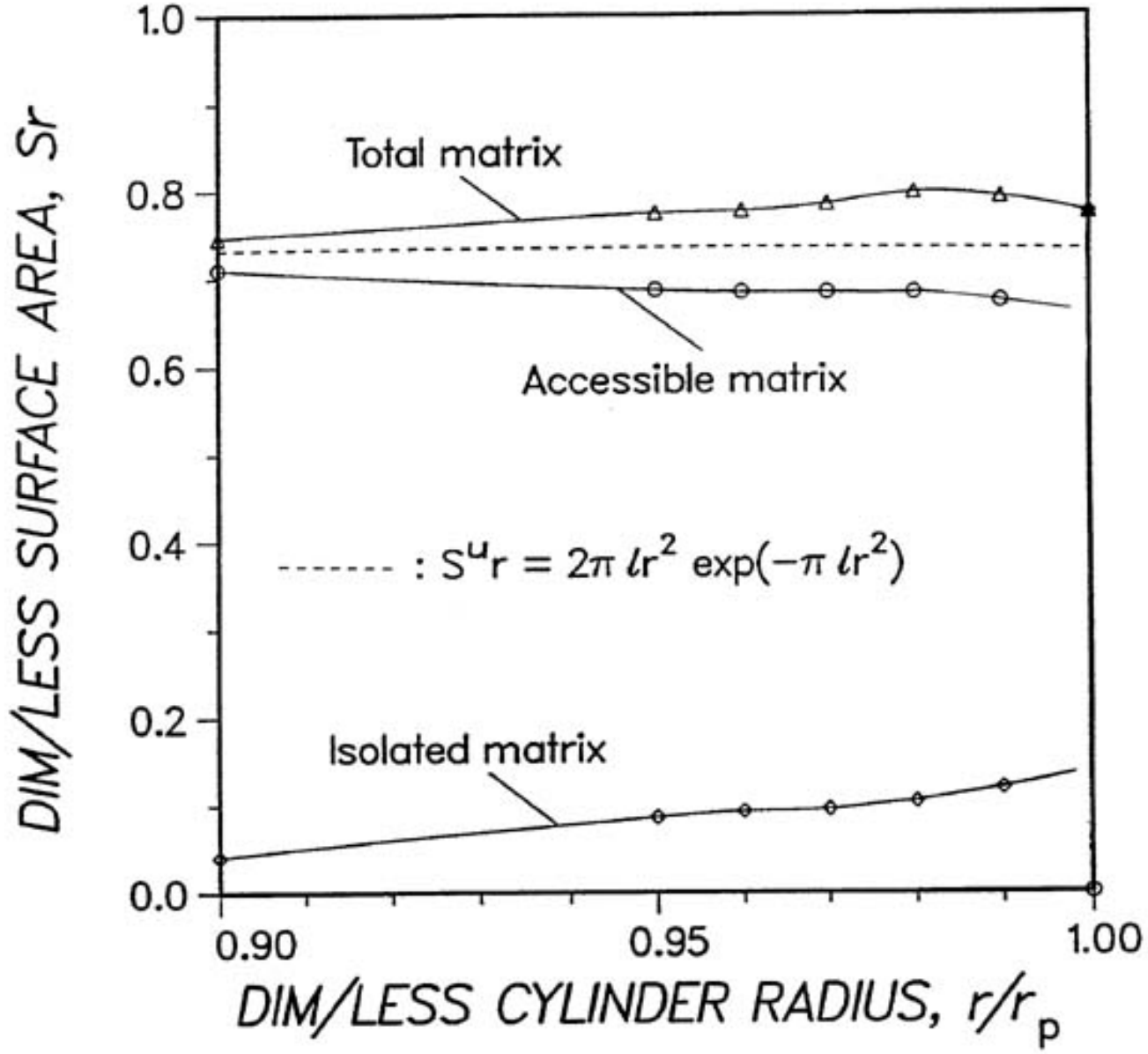


Figure 6. Variation of the dimensionless specific surface area with the particle growth in random arrays of fully penetrable, unidirectional cylinders. The dashed curve gives the total, dimensionless specific surface area for uniform particle growth.